AN EXPERIMENTAL INVESTIGATION OF GENERATION-RECOMBINATION NOISE IN DOUBLE-INJECTION DIODES

By

PETER RUDOLPH WORCH

Bachelor of Science
Union College
Schenectady, New York
1957

Master of Science
Oklahoma State University
Stillwater, Oklahoma
1965

Submitted to the Faculty of the Graduate College
of the Oklahoma State University
in partial fulfillment of the requirements
for the Degree of
DOCTOR OF PHILOSOPHY
May, 1970

AN EXPERIMENTAL INVESTIGATION OF
GENERATION-RECOMBINATION NOISE
IN DOUBLE-INJECTION DIODES

Thesis Approved:

Hans A. Bilger
Thesis Adviser

William J. Lewis

Wm. J. Hughes

Joanne Agneew

D. Durham
Dean of the Graduate College

ACKNOWLEDGEMENTS

I wish to express my most sincere gratitude to my thesis adviser, Professor Hans R. Bilger, for the original idea for this research and for his continual advice, encouragement and assistance throughout my doctoral studies.

I also wish to thank the other members of my graduate committee, Professors W. L. Hughes, W. J. Leivo and J. L. Agnew for their guidance during my studies.

My special thanks to Professor M-A. Nicolet of the California Institute of Technology for his hospitality, his guidance and his assistance here and during my trips to his laboratory at Cal. Tech. I gratefully acknowledge the financial support given the investigation by NASA Grant NGR 05-002-100 through Cal. Tech.

I also express my gratitude to the United States Air Force for granting this leave of absence and for their financial support during my doctoral program.

Finally, to my wife, Jeanette, without whose assistance, understanding and encouragement this endeavor would have been impossible, I give my warmest appreciation. To my children, Cynthia and Peter, Jr., my thanks for their patience and understanding.

TABLE OF CONTENTS

LIST OF TABLES

LIST OF FIGURES

CHAPTER I

INTRODUCTION

Background

Fluctuation phenomena in semiconductors may be defined (1) as the spontaneous fluctuations in current through, or voltage across, semiconductor devices. These fluctuations are commonly realized as noise in the circuitry to which the devices are applied, hence, the fluctuations themselves are more often termed "noise". The study of the fluctuation phenomena not only provides an understanding of the basic limitations on device operation (and hints on the improvement thereof) but also establishes an insight to the fundamental physics of semiconductor materials and devices. For these reasons, noise studies have appeared frequently in the literature in recent years. General textbooks on noise have been written by van der Ziel (2), Bennett (3), King (4), MacDonald (5) and others.

Three major noise sources predominate in semiconductor operation: thermal noise, flicker noise and generation-recombination noise. Thermal noise is due to fluctuations in the thermal velocity of current carriers in all resistive devices. It is also known as Nyquist noise after one of its early investigators (6) and likewise as Johnson noise (7). Flicker noise was studied by Williams and Thatcher (8) and later by Bernamont (9). Flicker noise (or 1/f noise as it is also known) in semiconductors is generally associated with surface and bulk leakage

effects near current-carrying contacts though little is known of its specific sources. Generation-recombination (g-r) noise, to which this dissertation is addressed, results from fluctuations in the current-carrier density. It was shown to exist by Herzog and van der Ziel (10) and has since been studied for a variety of materials, devices and conditions (11,12,13).

The double-injection diode (DID) is a relatively new semiconductor device which operates with the simultaneous injection of current-carrying electrons and holes from opposite ends of the device. Lampert and Rose (14) made the basic study of double injection in semiconductors and have predicted the direct current behavior. Since that time there have been numerous theoretical and experimental studies of the dc characteristics of double injection (15,16,17,18) and a few studies of the ac behavior and noise (19,20) in double-injection devices. A concise and complete history and discussion of double-injection theory has been compiled by Baron and Mayer (21).

The Problem

The generation-recombination noise of double-injection diodes has not yet been fully investigated. Those regimes of operation of the DID predicted by Lampert and Rose are clearly and separately realized only under very restricting conditions. Where the operating regime can be isolated and investigated, there exists the intriguing possibility of associating the mode or regime with the magnitude of the generation-recombination noise.

The major contribution of this thesis is the experimental investigation of g-r noise in a DID operating in the so-called Lampert

semiconductor regime and a comparison of the experimental results with the available theoretical predictions.

Scope of Investigation

A brief summary of the published developments in double-injection diode theory is given. Noise is discussed and the current theories for generation-recombination noise in the DID are presented.

Prerequisite to the experimental study of g-r noise is the construction of a device. The manufacture of a suitable DID was so important and so critical that a discussion of the process is warranted here. Of further significance is the development of the methods and procedures necessary to accurately measure and evaluate g-r noise. These too are discussed herein.

The actually-measured dc and ac behavior of the experimental DIDs is presented as well as the comparison of these results with current theories. Noise measurement results are given and their comparison with theory and the known device parameters is discussed.

CHAPTER II

THEORY OF GENERATION-RECOMBINATION NOISE IN A DOUBLE-INJECTION DIODE

The double-injection diode is a semiconductor structure with certain unique transport properties. Double injection means the simultaneous injection, from opposite ends of a n^+-π-p^+ (or n^+-ν-p^+) device, of electrons and holes. Under these conditions, space charge current limitations are reduced and recombination essentially limits the current flow. There has been a great deal of investigation into double-injection diodes, most of which is summarized by Baron and Mayer (21), so only a general presentation of that theory pertinent to the experimental work of this thesis is given here. A list of symbols is included as Appendix A.

DC and AC Behavior

The dc theory of the double-injection diode was summarized by Lampert and Rose (14) who showed that for the long structure case (negligible diffusion currents), three main modes of operation of the forward-biased diode occur. In the "ohmic" regime, conduction is due solely to thermally-generated carriers so the behavior is simply that of a resistor where $I \propto V$. At higher carrier injection levels, the current is carried by injected carriers but space charge effects are negligible and the "semiconductor" regime is reached where $I \propto V^2$. At

still higher injection levels, only injected carriers contribute to conduction and space charge effects become significant hence the "insulator" regime is attained where $I \propto V^3$.

Consider the simplified double-injection diode schematically shown in Figure 1.

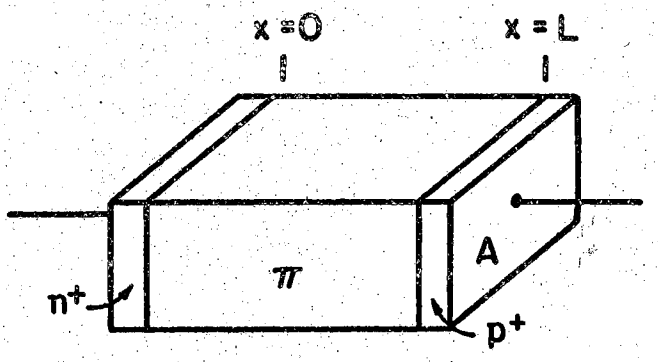

Figure 1. Schematic Representation of a Double-Injection Diode

The basis for the development is the set of transport equations,

$$\vec{J}_n = q\mu_n\left[(n_T + \delta n)\vec{E} + \frac{kT}{q}\vec{\nabla}\,\delta n\right] + \epsilon\epsilon_0\frac{\partial\vec{E}}{\partial t} \quad , \qquad (2.1)$$

$$\vec{J}_p = q\mu_p\left[(p_T + \delta p)\vec{E} - \frac{kT}{q}\vec{\nabla}\,\delta p\right] + \epsilon\epsilon_0\frac{\partial\vec{E}}{\partial t} \quad , \qquad (2.2)$$

$$\vec{J} = \vec{J}_n + \vec{J}_p \quad . \qquad (2.3)$$

The device is assumed to be homogeneous with single-dimensional behavior. Then the particle conservation equations may be written as

$$-\frac{\partial n}{\partial t} + \frac{1}{q}\frac{\partial}{\partial x}J_n = r \quad , \qquad (2.4)$$

$$\frac{\partial p}{\partial t} + \frac{1}{q} \frac{\partial}{\partial x} J_p = - r \quad , \tag{2.5}$$

where Baron and Mayer (21) are followed using

$$r = \frac{\delta n}{\tau} \quad . \tag{2.6}$$

It is also necessary to use Poisson's equation,

$$\frac{\epsilon \epsilon_0}{q} \frac{\partial E}{\partial x} = \delta p - \delta n \quad . \tag{2.7}$$

Manipulation of these equations reduced to time independent form results in [see Lampert and Rose (14)] a master differential equation for double injection behavior,

$$(n_T - p_T) \frac{dE}{dx} - \frac{\epsilon \epsilon_0}{q} \frac{d}{dx} \left(E \frac{dE}{dx}\right) + \beta \frac{d^2}{dx^2} (\delta n + \delta p) = \frac{(b+1)\ \delta n}{\mu_n \tau} \quad . \tag{2.8}$$

Consider only the case of a long structure in which diffusion currents are negligible so that the diffusion term of Equation 2.8 (third term on the left) is dropped from further consideration. For the dc behavior, the result is

$$(n_T - p_T) \frac{dE}{dx} - \frac{\epsilon \epsilon_0}{q} \frac{d}{dx} \left(E \frac{dE}{dx}\right) = \frac{(b+1)\ \delta n}{\mu_n \tau} \quad . \tag{2.8a}$$

The reduced master differential equation (2.8a) still does not lend itself to closed-form solution though Lee (22) has computed numerical solutions. Using the following reasoning, the physical requirements for the three regimes of operation may be defined and it then becomes possible to obtain analytic solutions. If the spatial derivatives in the equation are considered as zero (constant electric field), both terms on the left drop out and the ohmic regime is established. Retaining the first term (relating to thermally-generated

carriers) and neglecting the second term defines the semiconductor regime of operation. If, on the other hand, the second term (space charge term) is kept and the first term dropped, the insulator regime is defined.

Specifically, the solution for the ohmic regime is

$$J = q\ \mu_p(b\ n_T + p_T)\ \frac{V}{L} \quad . \tag{2.9}$$

For the semiconductor regime, the differential equation is solved using the boundary condition $E(0) = 0$. This condition is justified by Baron and Mayer (21) as being due to the high density of mobile carriers near the heavily injecting n^+-π junction. It appears to be experimentally verified in potential probe measurements by Mayer et al. (18) as well as in our profile measurements (see Figure 12). The result is

$$J = \frac{9}{8}\ q\ \mu_n\mu_p(p_T - n_T)\ \tau\ \frac{V^2}{L^3} \quad . \tag{2.10}$$

In the insulator regime, the injected carrier density is very high and the high concentrations of mobile carriers at both junctions justify setting $E(0) = E(L) = 0$. The result is

$$J = \frac{125}{18}\ \mu_n\mu_p\ \tau\ \varepsilon\varepsilon_0\ \frac{V^3}{L^5} \quad . \tag{2.11}$$

For the ac behavior of the double-injection diode, it is necessary to consider the time dependent master differential equation. The development of a completely general relation is very involved, however, so the approach of Driedonks and Zijlstra (20) is used and immediately diffusion and displacement currents are neglected. The basic current and continuity equations combine to give the time dependent master equation (mixed partials are neglected),

$$(n_T - p_T)\frac{\partial E}{\partial x} - \frac{\epsilon\epsilon_0}{q}\frac{\partial}{\partial x}\left(E\frac{\partial E}{\partial x}\right) - \frac{1}{q\mu_n\mu_p}\frac{\partial}{\partial t}\left(\frac{J}{E}\right) = \frac{(b+1)\delta n}{\mu_n \tau} \quad . \quad (2.12)$$

The ac response is obtained by introducing the electric field and current density as sums of dc and sinusoidal ac terms:

$$E = E_0 + \tilde{e}$$
$$J = J_0 + \tilde{j} \quad . \quad (2.13)$$

After Equation 2.12 is reduced for the specific regime of concern, Equations 2.13 are substituted and the resulting equation is "linearized" by removing higher power and combination terms in $\tilde{e}$, $\tilde{j}$ and their derivatives. Upon simplification with the dc field relationship for the semiconductor regime,

$$\tilde{e} = \frac{\tilde{j}}{J_0}\left(\frac{1 + i\omega\tau}{2 + i\omega\tau}\right) E_0 \quad .$$

The admittance is then given by

$$Y(\omega) = \frac{\tilde{i}}{\tilde{v}} = \frac{\tilde{j}A}{\int \tilde{e}\, dx} = \frac{I_0}{V_0}\frac{2 + i\omega\tau}{1 + i\omega\tau} \quad . \quad (2.14)$$

For the insulator regime it can be similarly found that the admittance is then

$$Y(\omega) = \frac{I_0}{V_0}\frac{3 + i\omega\tau}{1 + i\omega\tau} \quad . \quad (2.15)$$

The equivalent circuit associated with Equations 2.14 and 2.15 is shown in Figure 2. Circuit values in the accompanying table are obtained directly by analysis of the equations. This circuit is considered (19,23) as the low-frequency circuit. It is valid up to

frequencies of the order of the reciprocal dielectric relaxation time (in this case, greater than 10^7 Hz). For a further study of the high frequency circuit where capacitance effects must be considered, see Lee (23).

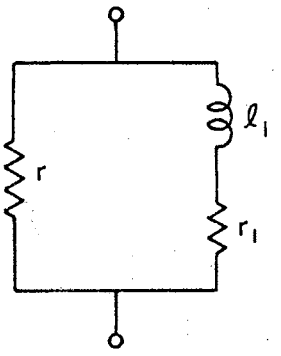

	Ohmic	Semiconductor	Insulator
r	$\frac{V_0}{I_0}$	$\frac{V_0}{I_0}$	$\frac{V_0}{I_0}$
r_1	∞	r	$\frac{r}{2}$
ℓ_1	—	$r_1\tau$	$r_1\tau$

Figure 2. Equivalent Circuit of a Double-Injection Diode

The carrier density and electric field profiles have been presented for the insulator regime (15) and both theoretically (17,23) and experimentally (18) for the semiconductor regime. In the case of the Lampert semiconductor regime, the analytic solution of the master differential equation (Equation 2.8a) provides an explicit equation for the magnitude of the electric field in the π region of an n^+-π-p^+ diode,

$$E = \left(\frac{2J}{q\mu_n\mu_p p_T \tau}\right)^{\frac{1}{2}} x^{\frac{1}{2}} \quad . \tag{2.16}$$

This, in turn, is used to generate an equation for the carrier density,

$$\delta n = \delta p = \left[\frac{J\, b\, \tau\, p_T}{2\, q\, (b+1)^2}\right]^{\frac{1}{2}} x^{-\frac{1}{2}} \quad . \tag{2.17}$$

Equations 2.16 and 2.17 apply for that case in which diffusion is neglected. Diffusion may be neglected for $L \gg L_a$ where L_a is the ambipolar diffusion length defined by

$$L_a = \left(\frac{2\beta\mu_n\tau}{b+1}\right)^{\frac{1}{2}} \quad . \tag{2.18}$$

Lee (22) has provided the results of a numerical solution to the master differential equation in which diffusion effects are retained. For an n^+-π-p^+ diode in which $p_T = 1.1 \times 10^{18}\ m^{-3}$, $\tau = 40\ \mu s$ and $T = 300^\circ$ K, the results are shown in Figures 3 and 4. Superimposed on Figure 4 is the carrier density distribution for the analytic solution (Lampert's solution) of the differential equation at the current density of $J = 10\ A/m^2$. It can be seen that the effects of diffusion are indeed restricted to the immediate vicinity of the junctions.

Generation-Recombination Noise

Semiconductors operated as double-injection diodes are known to exhibit, in general, three main components of noise: the so-called 1/f or flicker noise, generation-recombination noise and thermal or Nyquist noise. Each of these has been briefly discussed in the introductory chapter. The magnitude of each of the component noises is, of course, dependent on physical geometry and electrical parameters but a reasonable composition might appear as shown in Figure 5. The total is the quadratic sum of the components. It is the generation-recombination noise this research investigates and hence every precaution was taken to cause that component to predominate in the devices constructed. The

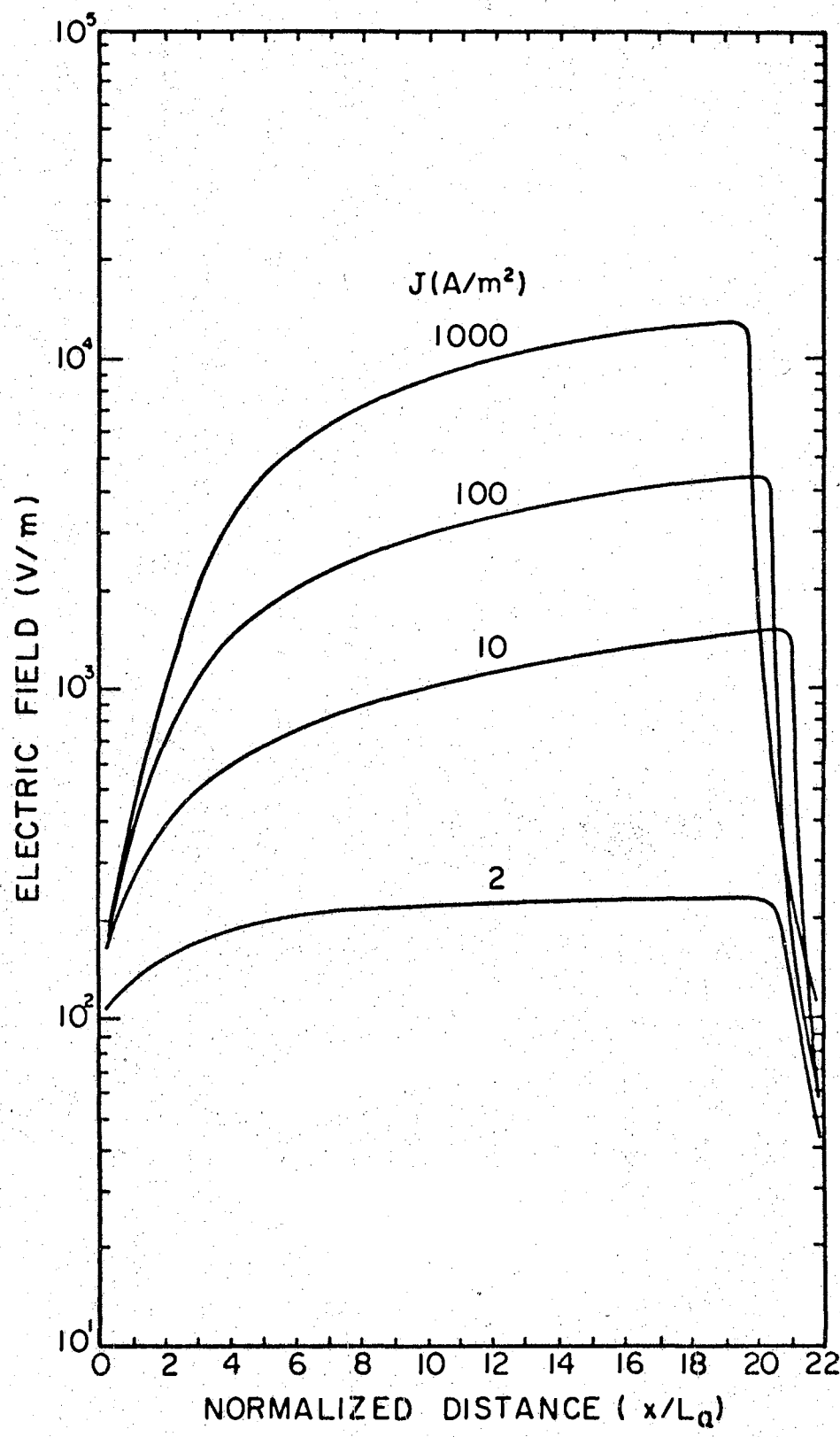

Figure 3. Electric Field Profile for an n^+-π-p^+ Diode

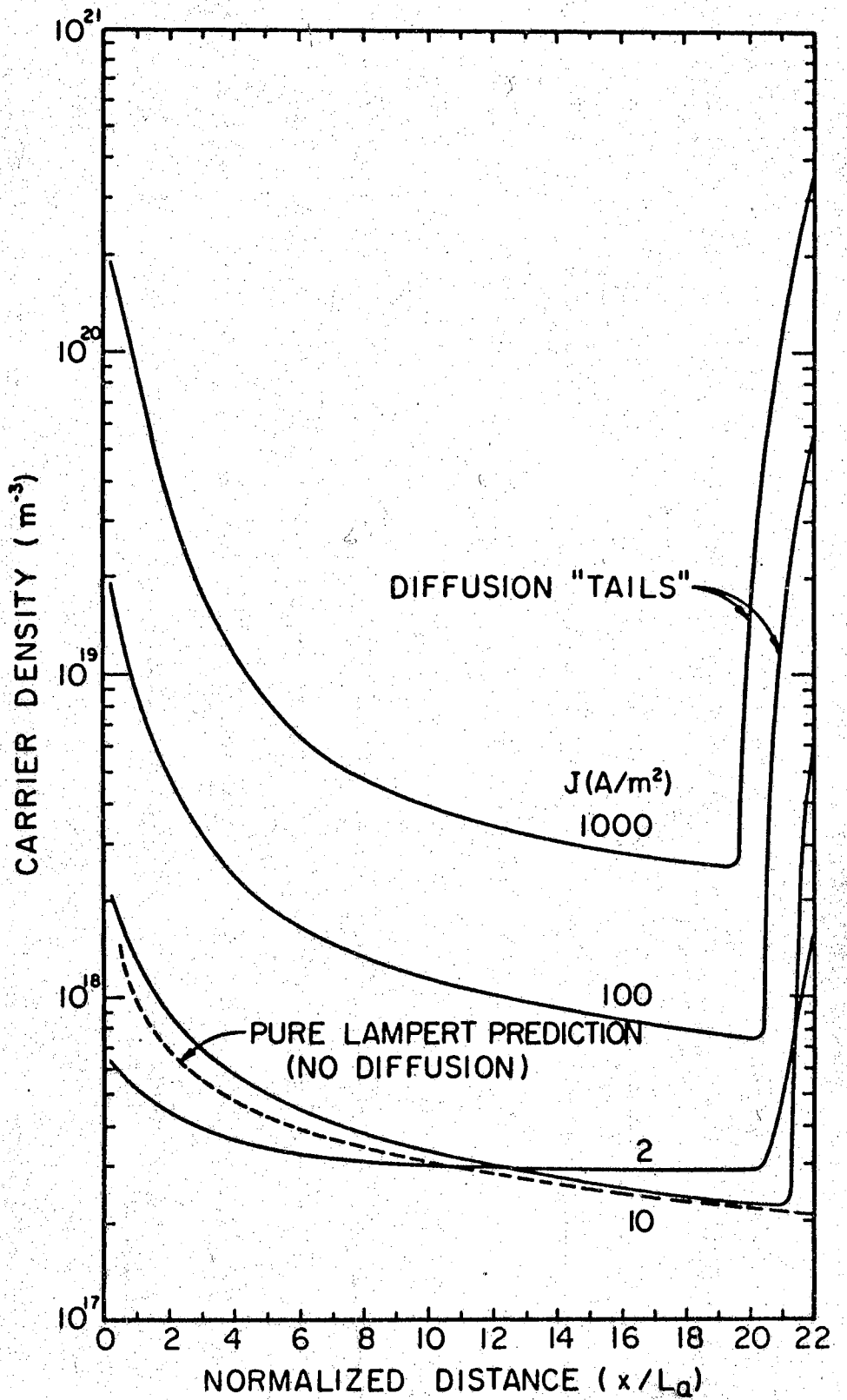

Figure 4. Carrier Density Profile for an n^+-π-p^+ Diode

flicker noise is the most difficult to control or to predict since a complete and sound theory of this noise has not been developed. Though the thermal noise of the semiconductor device is present in the measurements, this noise has been shown (19) to be just the thermal noise of the high frequency admittance given by Equation 2.14, which is easily accounted for.

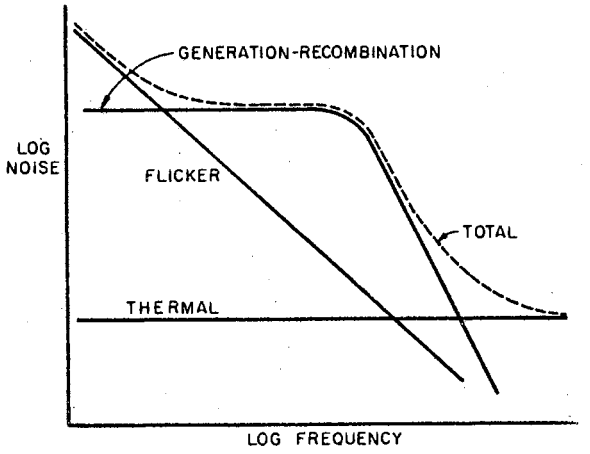

Figure 5. Noise in Semiconductors

Three different approaches to the g-r noise theory problem are significant in the literature and thus are discussed briefly here.

Lee Theory

The generation-recombination (g-r) noise in semiconductor materials was studied in detail by Van Vliet (24) and by Hill and Van Vliet (11),

both studies being based on a prediction of the variance of the fluctuations by Burgess (25,26). The Shockley-Read model (27) for the recombination process is used. A summary of the development of g-r noise theory for a homogeneous semiconductor crystal in equilibrium is also presented by van der Ziel (1).

van der Ziel considers an exponential distribution of lifetimes in the application of the Wiener-Khintchine theorem for the spectral density of a real causal function,

$$S(f) = 4 \int_0^\infty R(\tau) \cos 2\pi f\tau \, d\tau \quad ,$$

where $R(\tau)$ is the autocorrelation function. The relation for the variance $\overline{\Delta P^2}$ in fluctuations in the total number of carriers P devised by Burgess,

$$\overline{\Delta P^2} = \frac{PN}{P + N} \quad , \tag{2.19}$$

is used. The solution for the noise current spectral density of a homogeneous semiconductor crystal is

$$S_i(f) = \frac{4I^2 (b + 1)^2 n_T p_T \tau}{AL (bn_T + p_T)^2 (n_T + p_T) (1 + \omega^2\tau^2)} \quad . \tag{2.20}$$

Equation 2.20 applies specifically only to the case of a homogeneous semiconductor crystal in which current behaves linearly with applied voltage. The double-injection diode is linear only in the ohmic regime thus it is necessary to determine a satisfactory extension of theory to the case of a non-linear device. Lee (22) and Bilger et al. (28) have theorized that one can treat the double-injection diode as a series of differential slices, each of which can, for noise

purposes, be considered a linear device of length Δx and resistance ΔR. Further, as generation-recombination noise sources, these slices can be represented as ideal noise voltage generators in series with ideal resistances ΔR. The total noise is obtained by taking the quadratic sum of the noise voltage generators acting on the total ac resistance of the device. Mathematically then, the noise current spectral density of the slice is[1]

$$\Delta S_i(f) = \frac{4I^2}{A\Delta x} \frac{(b+1)^2}{(bn+p)^2} \frac{np}{n+p} \frac{\tau}{1+\omega^2\tau^2} \quad . \tag{2.21}$$

The resistance of the differential slice is defined as[2]

$$\Delta R = \frac{\psi(x+\Delta x) - \psi(x)}{\Delta I} = -\frac{\partial E}{\partial I} \Delta x \quad , \tag{2.22}$$

and the noise voltage contribution of that slice is

---

[1]It is assumed that the variance of the carrier density fluctuations for a near-intrinsic material with no excess carriers (as developed by Burgess),

$$\overline{\Delta P^2} = \frac{N_T P_T}{N_T + P_T} = \frac{n_T p_T}{n_T + p_T} AL \quad ,$$

can be extended to the case of high injection levels,

$$\overline{\Delta P^2} = \frac{np}{n+p} AL$$

where

$$n = n_T + \delta n$$

and

$$p = p_T + \delta p \quad .$$

[2]Lee actually used the definition,

$$\Delta R = \frac{\Delta V}{I} \quad .$$

This definition would increase the resultant noise current spectral density for the semiconductor regime by a factor 4. It has since been determined that Equation 2.22 provides a more realistic definition.

$$\Delta S_v(f) = \Delta S_i(f)\ (\Delta R)^2 \quad . \tag{2.23}$$

The noise fluctuations in individual slices are considered uncorrelated so the voltage contributions over the device are summed (by integration) and the resulting voltage spectral density is converted back into a current spectral density through

$$S_i(f) = S_v(f)\ (\frac{\partial I}{\partial V})^2 \quad .$$

Lee then gets as the basic noise current spectral density relation for semiconductor devices,

$$S_i(f) = 4\ (\frac{\partial I}{\partial V})^2\ \frac{(b+1)^2\tau I^2}{A(1+\omega^2\tau^2)} \int_0^L \frac{n(x)p(x)}{n(x)+p(x)}\ \frac{(\partial E/\partial I)^2}{[bn(x)+p(x)]^2}\ dx \quad . \tag{2.24}$$

To evaluate this relation for the case of a double-injection diode, the analytic solutions of the master differential equation for the electric field and carrier density ($n(x) = p(x) = \delta n$) in a p material (Equations 2.16 and 2.17) are applied and Equation 2.24 is integrated over the length of the near-intrinsic region of the device. Then the noise current spectral density for a double-injection diode operating in the semiconductor regime is

$$S_i(f) = \frac{9\sqrt{2}}{5}\ \frac{b+1}{1+\omega^2\tau^2}\ (\frac{q\ \tau}{b\ \mu AL|n_T-p_T|})^{\frac{1}{2}}\ I^{3/2} \quad . \tag{2.25}$$

This noise current spectral density may be converted to an equivalent shot noise diode current;

$$I_{eq} = \frac{S_i(f)}{2q} = \frac{9\sqrt{2}}{10}\ \frac{b+1}{1+\omega^2\tau^2}\ (\frac{\tau}{bqAL|n_T-p_T|})^{\frac{1}{2}}\ I^{3/2} \quad . \tag{2.26}$$

For the case of a DID of π material operating in the insulator

regime, it is necessary to apply the change of variables (20),

$$\frac{d}{dy} = E \frac{d}{dx} \quad .$$

In this case,

$$n = \delta n = \frac{1}{b+1} \left(\frac{J}{q \mu_p E} - \frac{\epsilon\epsilon_0}{q E} \frac{dE}{dy} \right) \quad ,$$

$$p = \delta p = \frac{1}{b+1} \left(\frac{J}{q \mu_p E} + \frac{b\epsilon\epsilon_0}{q E} \frac{dE}{dy} \right) \quad ,$$

and the electric field is given by

$$E = \frac{a}{2} y(y - y_L) \quad ,$$

where

$$y_L = y(x = L) = -\left(\frac{12L}{a}\right)^{1/3}$$

and

$$a = - \frac{J}{\mu_p \mu_n \tau \epsilon\epsilon_0} \quad .$$

The relation for noise current spectral density, Equation 2.24, is again evaluated. The result, expressed as an equivalent shot noise current, is

$$I_{eq} = \frac{30}{7} \left(\frac{1}{18}\right)^{2/3} \frac{b+1}{1+\omega^2\tau^2} \left(\frac{\tau^2 \mu_p}{bAL\epsilon\epsilon_0}\right)^{1/3} I^{4/3} \quad . \qquad (2.27)$$

Driedonks Theory

There has been another approach to noise theory used for many years and this method is known as the Langevin Analysis. Langevin (29)

introduced an analysis of Brownian movement which could be applied to the macroscopic differential equation of the system. The system, while originally mechanical, could as well be an electrical circuit. Using this approach, the statistics of the fluctuations provide sufficient information as to the nature of those fluctuations in order to solve for the mean square noise voltage (or current). Driedonks (30) has applied the Langevin approach to the double-injection diode by simply adding a noise source term H(x,t), with the appropriate statistical properties, to the basic ac equations for the device. By this method, Driedonks argues, though the noise sources are considered spatially independent, the correlation of fluctuations in different cross sections is taken into account. This aspect is the main difference between his theory and that of Lee. Under essentially the same development used earlier in this chapter, Driedonks introduces the carrier density fluctuation rate term H(x,t) into the continuity equation and gets for his master differential equation[3],

$$(n_T-p_T)\frac{\partial E}{\partial x} - \frac{\epsilon\epsilon_0}{q}\frac{\partial}{\partial x}\left(E\frac{\partial E}{\partial x}\right) - \frac{1}{q\mu_n\mu_p}\frac{\partial}{\partial t}\left(\frac{J}{E}\right) = \frac{(b+1)}{\mu_n}H(x,t)$$

$$+ \frac{J}{q\mu_n\mu_p\tau E} - \frac{n_T\mu_n + p_T\mu_p}{\mu_n\mu_p\tau} \quad . \qquad (2.28)$$

The solution of this equation for the noise involves the same analytic approximations previously used for the dc case. On the left side of the equation, only the third term is retained for the ohmic regime, the first and third are retained for the semiconductor regime and the

---

[3]Equation 2.28, without the noise source term and under the assumption that $\delta n = \delta p$, is just the ac or time dependent master equation (Equation 2.12) discussed earlier.

second and third terms are retained for the insulator regime. The third term on the right side is retained only for the ohmic regime case. Applying Fourier techniques to solve the partial differential equation, Driedonks gets the same result previously devised for the ohmic regime (see Equation 2.20). For the semiconductor and insulator regimes,

$$I_{eq} = \frac{3\sqrt{2}}{5} \frac{b+1}{1+\omega^2\tau^2} \frac{1 + \frac{\omega^2\tau^2}{4}}{1 + \frac{\omega^2\tau^2}{16}} \left(\frac{\tau}{bqAL|n_T - p_T|}\right)^{\frac{1}{2}} I^{3/2} \quad , \qquad (2.29)$$

and

$$I_{eq} = \frac{30}{7} \left(\frac{1}{18}\right)^{2/3} \frac{b+1}{1+\omega^2\tau^2} \left(\frac{\tau^2 \mu_p}{bAL\epsilon\epsilon_0}\right)^{1/3} I^{4/3} \quad . \qquad (2.30)$$

Fazakas Theory

Fazakas and Friedman (31) have used still another approach called the Lax Method and obtained an extremely complex relation which will not be presented here. They did show that at low frequencies (the plateau), the noise current spectral density for the semiconductor regime is given by

$$S_i(f) \propto \frac{I^2\tau}{N + P} \quad . \qquad (2.31)$$

When the current is considered a drift current and the total carrier density is assumed to be that of the injected carriers, the equivalent shot noise current is given by

$$I_{eq} \propto (b+1) \left(\frac{\tau}{bqAL|n_T - p_T|}\right)^{\frac{1}{2}} I^{3/2} \quad . \qquad (2.32)$$

At high frequencies, their relation becomes proportional to $\omega^{-3/2}$ with

periodic humps[4].

It should be noted that in their development, Fazakas and Friedman do not separate the high injection case into a "semiconductor regime" and an "insulator regime". This research treats only the theory's applicability to the Lampert semiconductor regime case.

Summary

Table I provides a summary of the theoretical dc, ac and noise behavior.

---

[4]A later correspondence from V. Sergiescu (32), an associate of Fazakas and Friedman, refuted the existence of these humps or oscillations in the predicted spectra.

TABLE I

THEORY SUMMARY

	OHMIC REGIME	SEMICONDUCTOR REGIME	INSULATOR REGIME
Carrier Condition	$n = n_T$ $p = p_T$	$n = \delta n$ $\delta n = \delta p$ $p = \delta p$	$n = \delta n$ $\delta n \neq \delta p$ $p = \delta p$
J	$q\mu_p(bn_T+p_T)\ \frac{V}{L}$	$\frac{9}{8}\ q\mu_n\mu_p(p_T-n_T)\tau\ \frac{V^2}{L^3}$	$\frac{125}{18}\ \mu_n\mu_p\ \tau\ \epsilon\epsilon_0\ \frac{V^3}{L^5}$
Y	$\frac{I_0}{V_0}$	$\frac{I_0}{V_0}\ \frac{2+i\omega\tau}{1+i\omega\tau}$	$\frac{I_0}{V_0}\ \frac{3+i\omega\tau}{1+i\omega\tau}$
Lee I_{eq}	$\frac{2(b+1)^2\ \tau\ n_T\ p_T}{ALq(1+\omega^2\tau^2)(n_T+p_T)(bn_T+p_T)^2}\ I^2$	$\frac{9\sqrt{2}}{10}\ \frac{(b+1)}{(1+\omega^2\tau^2)}\ \left(\frac{\tau}{bqAL\lvert n_T-p_T\rvert}\right)^{\frac{1}{2}}I^{\frac{3}{2}}$	$\frac{30}{7}\left(\frac{1}{18}\right)^{\frac{2}{3}}\frac{(b+1)}{(1+\omega^2\tau^2)}\left(\frac{\tau^2\ \mu_p}{bAL\epsilon\epsilon_0}\right)^{\frac{1}{3}}I^{\frac{4}{3}}$
Driedonks I_{eq}	$\frac{2(b+1)^2\ \tau\ n_T\ p_T}{ALq(1+\omega^2\tau^2)(n_T+p_T)(bn_T+p_T)^2}\ I^2$	$\frac{3\sqrt{2}}{5}\ \frac{(b+1)\left(1+\frac{\omega^2\tau^2}{4}\right)}{(1+\omega^2\tau^2)\left(1+\frac{\omega^2\tau^2}{16}\right)}\left(\frac{\tau}{bqAL\lvert n_T-p_T\rvert}\right)^{\frac{1}{2}}I^{\frac{3}{2}}$	$\frac{30}{7}\left(\frac{1}{18}\right)^{\frac{2}{3}}\frac{(b+1)}{(1+\omega^2\tau^2)}\left(\frac{\tau^2\ \mu_p}{bAL\epsilon\epsilon_0}\right)^{\frac{1}{3}}I^{\frac{4}{3}}$
Fazakas I_{eq}		$\propto (b+1)\ \left(\frac{\tau}{bqAL\lvert n_T-p_T\rvert}\right)^{\frac{1}{2}}\ I^{\frac{3}{2}}$ ($\propto \omega^{-3/2}$ at high freq.)	

CHAPTER III

EXPERIMENTAL ARRANGEMENTS AND PROCEDURES

Individually, the circuits and methods used for this research cannot be considered completely original, however the use of such equipment and the application of the methodology to test this type of semiconductor device for the ranges of parameters encountered is important enough and unique enough to be presented in some detail here. It is, of course, neither possible nor pertinent to discuss all the tests used but the major checks are included and others have a more detailed reference indicated. The dc measurements will not be discussed since the current-voltage checks were straight-forward and the potential probe measurements are explained by Mayer et al. (18).

Construction of Devices

The shape and size of the double-injection diodes were of prime importance in this investigation. The devices must be long compared to the ambipolar diffusion length in order to minimize the effects of diffusion, that is, the diffusion "tails" (see Figure 4) must be short compared to the length of the π region so that a pure drift current may be assumed in noise considerations. On the other hand, the longer length increases the device resistance imposing increasing difficulties in measurement steps. Secondly, smaller device lengths mean greater g-r noise (see Table I) and a lower dc point of transition from ohmic

to semiconductor regimes (compare Equations 2.9 and 2.10) making it easier to maintain high injection levels without device heating. After consideration of these facts, device lengths of approximately 6 mm were chosen. The ambipolar diffusion length for experienced lifetimes of the order of 50 microseconds is given by

$$L_a = \left(\frac{2\beta\mu_n\tau}{b+1}\right)^{\frac{1}{2}} \approx 0.2 \text{ mm} \quad . \tag{2.18}$$

Thus the device length is some 30 times the ambipolar diffusion length. Potential probe measurements along the length of the device indicate the lithium diffuses approximately 1 mm into the silicon and the aluminum alloys to a depth of about 0.1 mm. These regions are essentially low resistivity regions so the actual device length is reduced by about 1.1 mm and the ratio of effective device length to ambipolar diffusion length is cut to about 25. This is considered adequate for the pure drift approximation.

The cross-sectional area of the devices is also quite important. On one hand one would like to keep the area very small to reduce the device current and to increase the g-r noise (Equation 2.26). On the other hand, large areas decrease the device resistance making some measurements easier. The larger area also allows larger contacts which in turn reduces contact resistance (resistance from contact to the bulk) and lowers current density and hence the flicker noise. Further, the difficulty in handling the devices to fabricate junctions and contacts increases with small devices. Typically, cross-sectional areas of 4 to 9 mm^2 were chosen to optimize behavior.

Some experimentation was done with devices having "arms" across

which noise measurements were made to avoid flicker noise generated in the immediate vicinity of the junctions [see Bilger et al. (28)]. Only moderate success can be claimed since it appeared that those devices which were considered "bad" in terms of high flicker noise did not show a significantly cleaner noise spectrum at the side contacts versus the end contacts and the additional problems associated with corrective factors to the measurements outweighed the small advantage of such a device. Figure 6 shows the general shapes used.

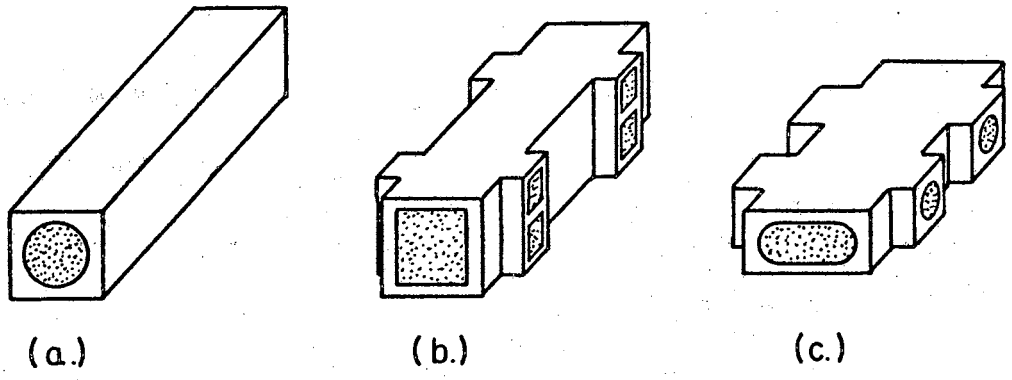

Figure 6. Device Shapes

Devices of the shape shown in Figure 6a were simply cut from the silicon slice with a diamond saw. Devices of the shapes of Figure 6b and 6c were shaped using an ultrasonic impact grinder (more detail is provided in Appendix B).

The material used for the devices was also chosen after careful consideration of the possible consequences. In general, one desires to minimize the current and maximize the noise hence it is obvious from

Table I that for the maximum g-r noise in the semiconductor regime one should use the purest material (lowest equilibrium carrier density) available. Lightly doped p (π) material was picked since this lowers the transition voltage by an additional factor of "b" over that of ν material. Though current is adversely affected, the increase in noise and the decrease in dc transition voltage indicate a long carrier lifetime is desireable. The devices, then, were usually made of high purity π type silicon (8.7 kΩcm to 200 kΩcm) material.

For the p^+ junction, aluminum was found to produce the most reproducibly good alloyed junction. For the n^+ junction, alloyed antimony-doped gold was repeatedly tried but never produced a good "square-law" device. In later devices, lithium was diffused into the silicon for the n^+ junction. Gold wire leads were soldered to the aluminum and gold alloy regions using 90% indium/10% silver solder. The lithium-diffused end was contacted by gallium friction-tinning and then applying a mound of indium-silver solder.

In later stages of device production, the DIDs were usually good in terms of ac and dc behavior. Unfortunately, the flicker noise characteristics varied quite widely with little correlation with material parameters or the method of preparation. At this time it is not possible to quote a recipe which will consistently produce double-injection diodes with low flicker noise, however, the recipe shown in Appendix B has proven 90% successful for producing devices with the predicted ac and dc characteristics.

Pulse Response Measurement

An elegant means of realizing and evaluating the ac equivalent circuit of the double-injection diode is through pulse response measurements (19). Basically, this consists of applying a small square voltage pulse of approximately 500 microseconds duration to the forward-biased diode and observing the resulting current pulse as shown in Figure 7.

Precautions were taken to keep leads short and otherwise minimize reactive effects. In this measurement, as in all electrical measurements of this research, the device was kept well-shielded from stray electrostatic fields and from light. The magnitude of the input pulse was small compared to the applied dc voltage to avoid non-linearities in the measurements.

Since the equivalent circuit of the DID indicates a series-parallel combination of resistors and inductors, the resulting current pulse is as shown in Figure 8. This pulse has the feature that the current response $\Delta i_1(t)$ is due to the "high frequency" resistance r while the response $\Delta i_2(t)$ is due to the build-up of charge carrier density in the bulk represented electrically by the series combination of r_1 and ℓ_1. For true Lampert semiconductor regime DID operation, $\Delta i_2(t)$ is just equal to $\Delta i_1(t)$ and the time constant τ is the carrier lifetime in the diode. The use of the Tektronix type W comparator plug-in unit and an oscilloscope with a calibrated triggering delay allows an expansion of the display and an accurate measurement of the current and lifetime.

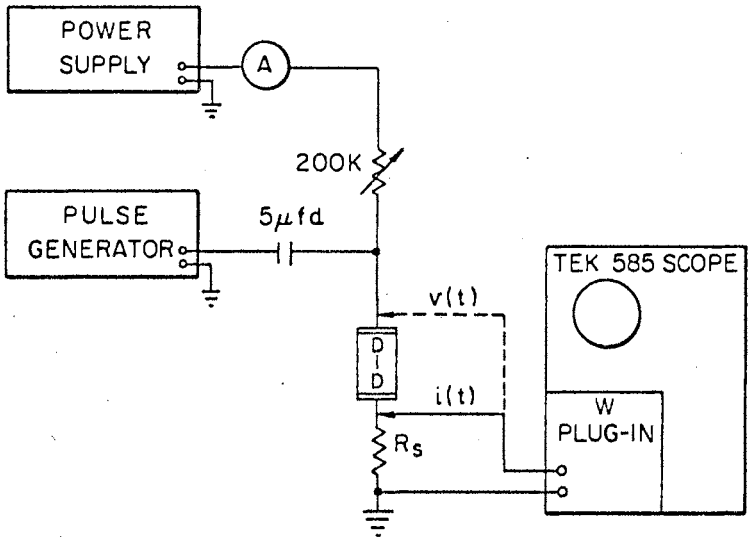

Figure 7. Pulse Response Circuit Layout

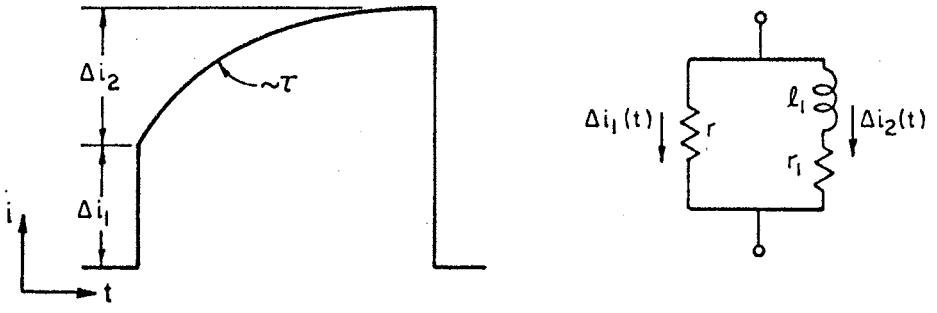

$$\Delta i(t) = \Delta i_1(0) + \Delta i_2(\infty) \left[1 - \exp(-t/\tau)\right]$$

Figure 8. Pulse Response of a Double-Injection Diode

Noise Measurement

The noise signals generated by the double-injection diodes are amplified and passed into a wave analyzer. The wave analyzer, used as a tuneable voltmeter, selects a narrow frequency band, filters and rectifies the signal and displays the result. Since large fluctuations on the rectified mean make interpretation of the needle reading difficult, especially at small filter bandwidths, the outputs were extracted at the recorder jacks, integrated and subsequently displayed on other instruments. A block diagram of the instrumentation is shown in Figure 9 and a photograph of the layout is provided as Figure 10.

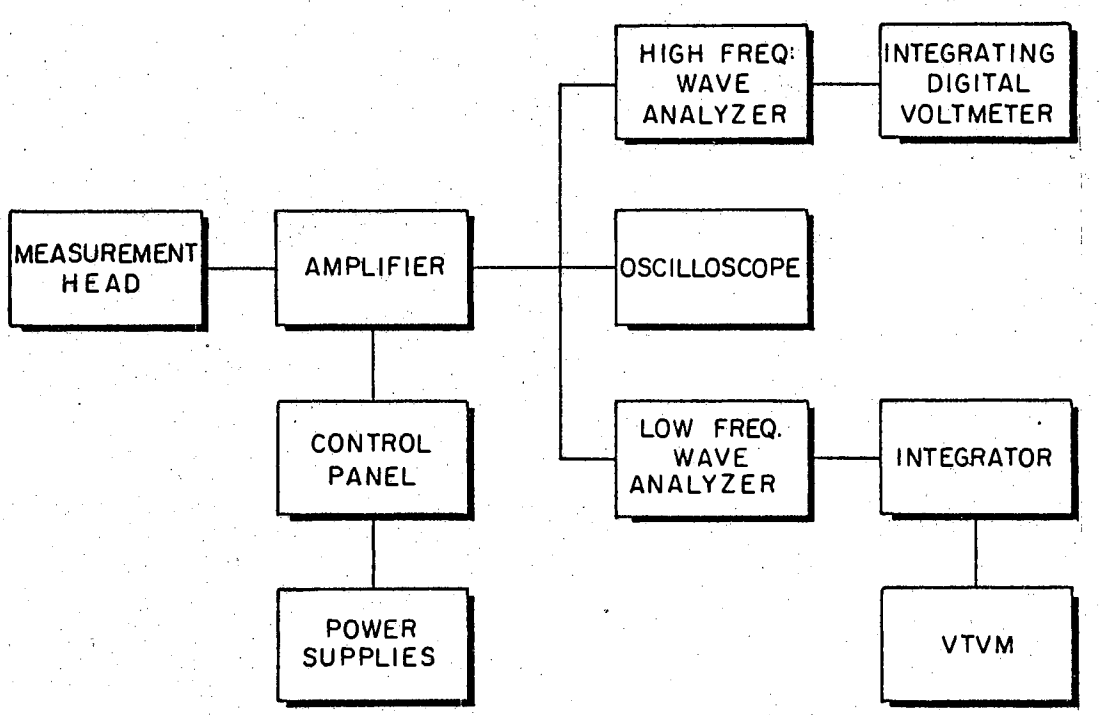

Figure 9. Noise Instrumentation Layout

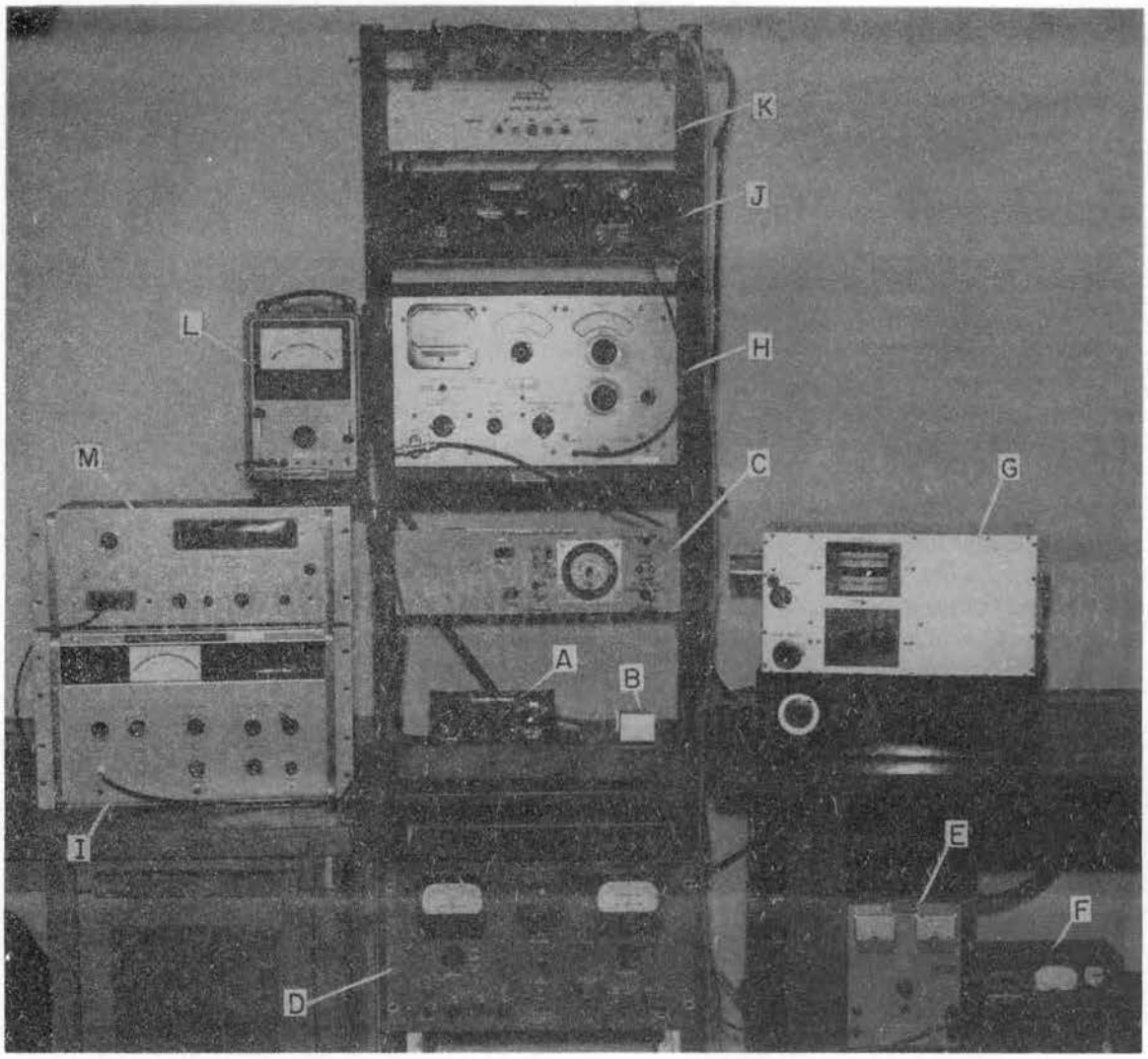

A - LOW FREQUENCY (LF) AMPLIFIER

B - MEASUREMENT HEAD (LF)

C - CONTROL PANEL (LF)

D - DEVICE POWER SUPPLY (LF)

E - NOISE TUBE FILAMENT SUPPLY (LF)

F - NOISE TUBE PLATE SUPPLY (LF)

G - HIGH FREQUENCY (HF) AMPLIFIER (INCLUDES HF EQUIVALENTS OF A-F)

H - WAVE ANALYZER (HP-302A)

I - WAVE ANALYZER (HO5-312A)

J - INTEGRATOR

K - INTEGRATOR POWER SUPPLY

L - VOLTMETER (HP 412A)

M - INTEGRATING VOLTMETER (HP 2401B)

Figure 10. Noise Measuring Apparatus

Two different noise amplifiers were used for the noise measurements, both having been developed for other noise research projects (12,23), but with minor modifications these were found quite suitable for measurement in this study. Details concerning their design are contained in the original documents so only a summary is presented here.

For the low frequency amplifier, a measured gain of 600 is achieved over the frequency range of interest (40 Hz to 1 MHz) through the use of two E810F Phillips (Amperex) tubes. A cathode follower then reduces the output impedance to approximately 70 ohms. A Sylvania type 5722 noise diode, used for calibration purposes, is included in the same cabinet with the amplifier. The high frequency amplifier is all solid-state (except for the type 5722 noise calibration diode). It has a gain of about 150 over the frequency range of 2 kHz to 22 MHz. A carefully selected low-noise FET (SF5868) is used for the input stage.

Two wave analyzers with considerable frequency overlap were used to cover the desired spectrum. For low frequencies, a Hewlett-Packard Model 302A wave analyzer with a 6 Hz bandwidth could be satisfactorily used from 20 Hz to 50 kHz. A Hewlett-Packard Model H05-312A wave analyzer was used for frequencies of 600 Hz and up (Its maximum frequency capability is 22 MHz). In this case a 200 Hz bandwidth was used.

As previously mentioned, the random needle fluctuations made meter observations difficult and errors large (see Appendix C), especially with the narrow bandwidth of the low frequency analyzer, so the rectified signals were fed to integrators. For the low frequency unit the signal was integrated, usually for 20 seconds, in a locally-developed integrator capable of 5, 10, 20, 50, and 100 second integration intervals. The result was then read from an HP 412A dc voltmeter. At

higher frequencies, it sufficed to feed the H05-312A analyzer output directly into an integrating digital voltmeter (Dymec Model 2401B) where a one second integration interval is used.

The measurement of the noise of devices such as these double-injection diodes or, for that matter, simple resistors turned out to be the most difficult portion of the entire research. The normally trivial problem of removing extraneous random or deterministic signals was most frustrating and accounted for many hours of orthodox and unorthodox experimentation.

A deterministic signal such as 60 Hz hum could be seen on the oscilloscope used to continuously monitor the amplifier output. In setting up the equipment, the hum originally seen was slowly reduced by experimenting with various equipment grounding combinations and with grounding in the amplifier. Shielding and bypassing meters helped reduce problems of magnetic pickup and the entire amplifier, measurement head and all cables were carefully shielded to minimize electrostatic pickup. Power supplies were selected for minimum hum and maximum isolation and additional filtering provided to further reduce hum. Even with all these precautions, operation of heavy ac equipment, rf generating equipment or other transient-producing equipment such as welders in and around the building forced a halt to measurement runs. Further, acoustic noises (doors, bells, loud talking) mechanically coupled into the amplifier tubes making some measurements (integration cycles) invalid. Either the oscilloscope or the large variation of a single reading was a warning to re-measure that point.

In the case of random noise, however, neither the scope nor the data analysis always helped in identifying a problem. Fortunately,

the method of calibration of the noise signal provided a means (theoretically) to overcome the problems of random noises due to external or internal sources. As a bonus, this calibration method removed the effect of amplifier gain variation with frequency.

Noise Calibration Method

The calibration procedure for noise measurements used a temperature-limited diode (Sylvania 5722) whose shot noise output is given by

$$\overline{I^2} = 2qI_c\Delta f \quad . \tag{3.1}$$

The noise is calibrated in terms of an equivalent shot noise current i.e., the dc current through a temperature-limited diode whose noise equals the measured noise. To do this it is necessary to make three noise measurements as follows:

a. Measure the mean square noise voltage output of the amplifier $(\overline{V_s^2})$ with the input short-circuited. This corresponds to the total noise of the amplifier.

b. Measure the mean square noise voltage output of the amplifier $(\overline{V_1^2})$ with the device connected to its input. This corresponds to the quadratic sum of the amplifier and device noises.

c. Measure the mean square noise voltage as in b, but with a filament voltage applied to the noise calibrator diode (connected to the amplifier input). This corresponds to the sum of noises of the amplifier, device and calibrator diode whose plate current I_c is also now recorded.

The noise due to the device is $\overline{V_1^2} - \overline{V_s^2}$. The noise due to the

calibration diode with dc current I_c is $\overline{V_2^2} - \overline{V_1^2}$. Hence the equivalent noise current of the DID is given by

$$I_{eq} = \frac{\overline{V_1^2} - \overline{V_s^2}}{\overline{V_2^2} - \overline{V_1^2}} I_c \quad . \tag{3.2}$$

The non-zero admittance of the amplifier input circuitry also produces thermal noise which enters into I_{eq} and thus a correction factor is necessary. This noise can be accounted for in the resulting spectra or by using a correcting I_{eq} designated $I_{eq\ z}$ which has been determined by measuring the equivalent noise current with an "open" input circuit. Equation 3.2 then becomes

$$I_{eq} = \frac{\overline{V_1^2} - \overline{V_s^2}}{\overline{V_2^2} - \overline{V_1^2}} I_c - I_{eq\ z} \quad . \tag{3.3}$$

Equation 3.3 is the basic equation used for reducing experimental noise data. The voltages V_s, V_1 and V_2 were read 3-6 times at each frequency point as outlined above and the average of the readings fed into Equation 3.3 which was programmed into a Hewlett-Packard 9100A desk calculator.

CHAPTER IV

EXPERIMENTAL RESULTS AND COMPARISON WITH THEORY

This chapter explains the experimental results of this investigation. The ac and dc behavior are as predicted and though the 1/f component of noise is higher than was hoped or anticipated, the noise due to the generation and recombination of carriers is clearly identifiable. Further, the current dependence of the g-r noise is essentially as expected though the transition from ohmic to semiconductor regimes as indicated by noise measurements occurs at a somewhat higher device current than that indicated by the dc behavior data. Significantly, however, the transition point or region defined by the noise vs device current data is just that indicated by the ac behavior. It should be noted that all theoretical calculations are based on the physical parameters summarized at the end of this chapter using the average pulse-measured figure for the carrier lifetime.

Diode 69-15

DC Behavior

The current-voltage characteristic for a double-injection diode (diode 69-15) appears in Figure 11. This diode was cut from Ingot "A" (see Appendix B) in the shape of Figure 6a. At low currents, junction potentials and contact drops cause an apparent increase in the curve slope over that expected of ohmic behavior. This has been encountered

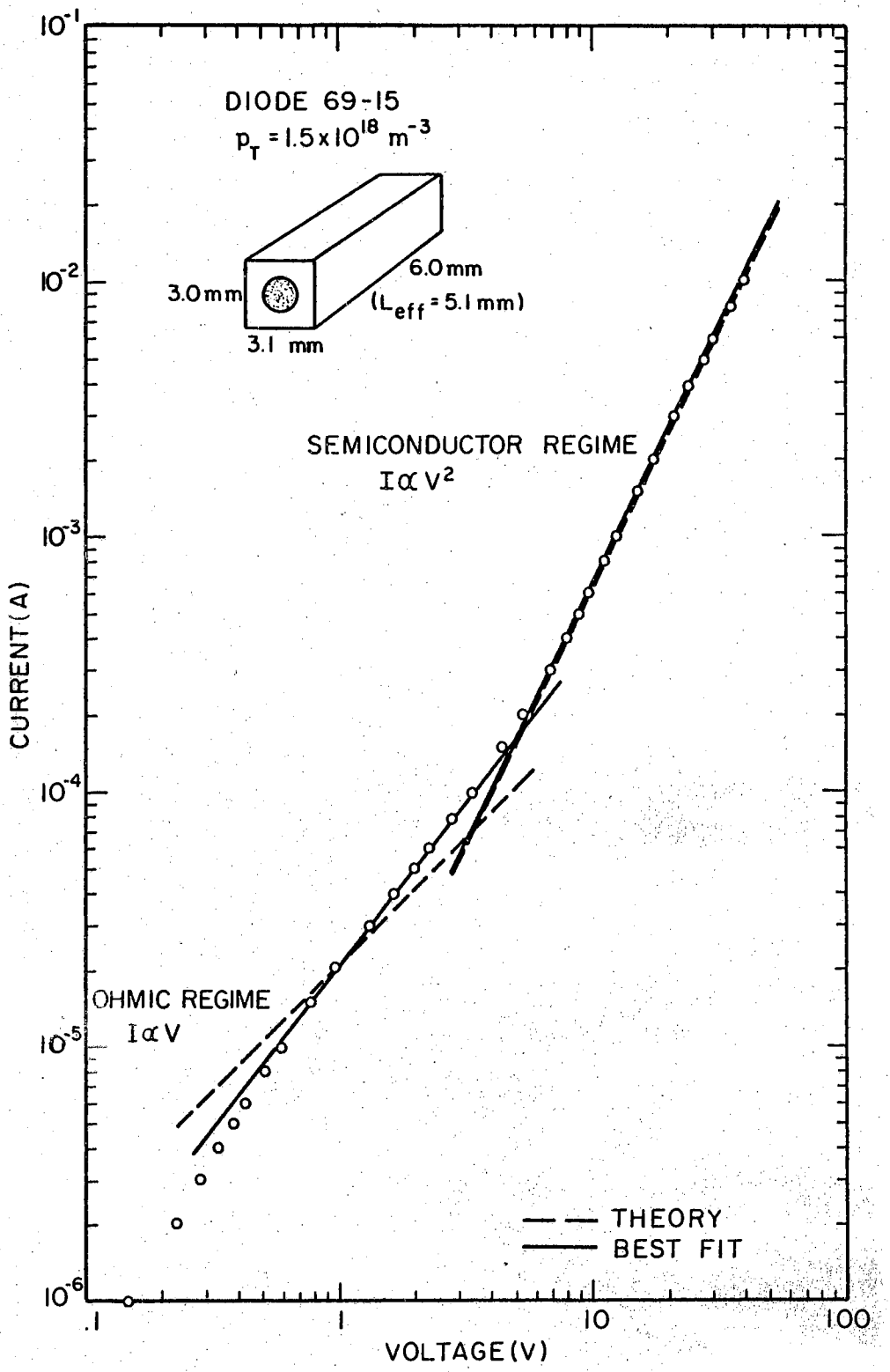

Figure 11. Current-Voltage Characteristic - Diode 69-15

by others (18) and is not considered significant. The true transition to the semiconductor regime is difficult to determine from the dc characteristics. There is an obvious crossing of asymptotes on the I-V plot (hereafter called the dc transition point), however as Baron (17) has predicted, this need not be that point where high level injection, the requirement for true Lampert semiconductor regime operation, occurs. In the semiconductor regime the slope on the log-log plot is 2.0 and while many diodes were constructed which exhibited this 2.0 slope, many others were also constructed which had lower slopes, typically 1.5 to 2.0. These diodes of lower "semiconductor regime" slopes were sometimes very clean of flicker noise, very clearly showing g-r noise and some even demonstrated other features indicative of double injection. The absence of the square-law I-V characteristic, however, made the consideration of other devices more desireable.

Figure 11 includes the theoretical current-voltage relationship for the semiconductor regime at a lifetime of 45 μs. It can be seen that in the semiconductor regime excellent agreement between theoretical and experimental results is obtained. The discrepancy between theory and experiment for the ohmic regime is assumed to be due to junction effects.

The device was next subjected to a dc potential probe. For this measurement, one longitudinal face of the diode was lapped with 3200 mesh grinding compound and the device mounted and biased into the semiconductor regime of operation. A tungsten probe measured the potential at points across the surface for the primary purpose of establishing the effective device length. Figure 12 displays a resulting potential probe measurement for a device current of 1 mA. The solid line

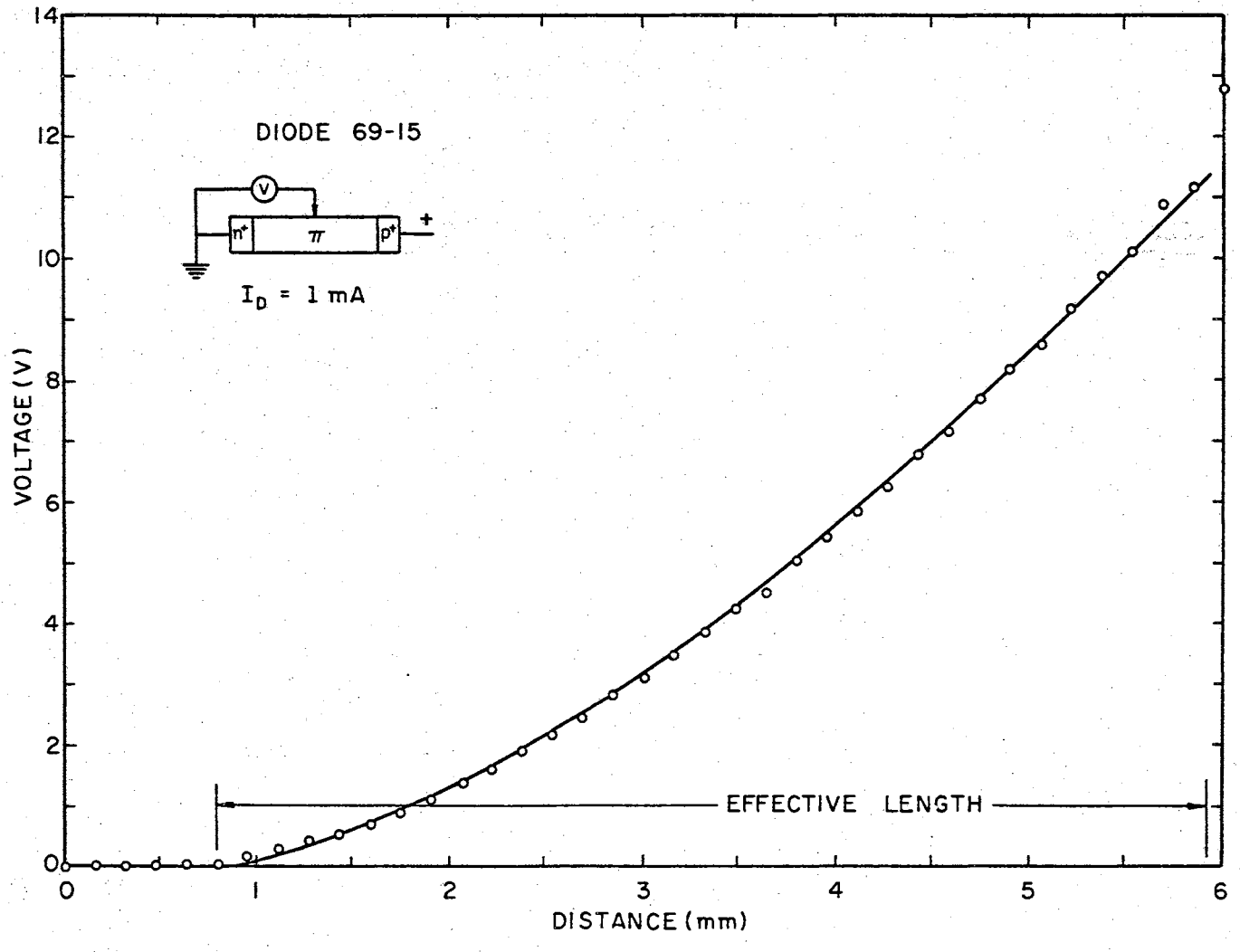

Figure 12. Potential Probe Measurement - Diode 69-15

represents a computed best curve fit of the analytic solution of the master differential equation (integral of the electric field given by Equation 2.16),

$$V = \frac{2}{3} \left(\frac{2J}{q\mu_n \mu_p p_T \tau}\right)^{\frac{1}{2}} x^{\frac{3}{2}} \quad . \tag{4.1}$$

At the n^+-π junction, a long region of negligible voltage defines the distance of the diffusion of the lithium. After this region, the measured values of voltage closely follow the theoretical curve until junction effects take over near the other end. As a secondary benefit, this measurement provides a crude determination of the carrier lifetime through Equation 4.1 (crude because it relates only to a portion of the total device length). In this case, lifetimes of the order of 60-70 microseconds were deduced, compared with pulse response lifetimes of 40-50 microseconds. The effective length vs current, shown in Figure 13, demonstrates the expected (17) decrease in effective length with current however the error involved in the length determination is 5% and this is already of the order of the actual change in length. The device length used for all calculations pertaining to the semiconductor regime was taken as 5.1 mm from this measurement.

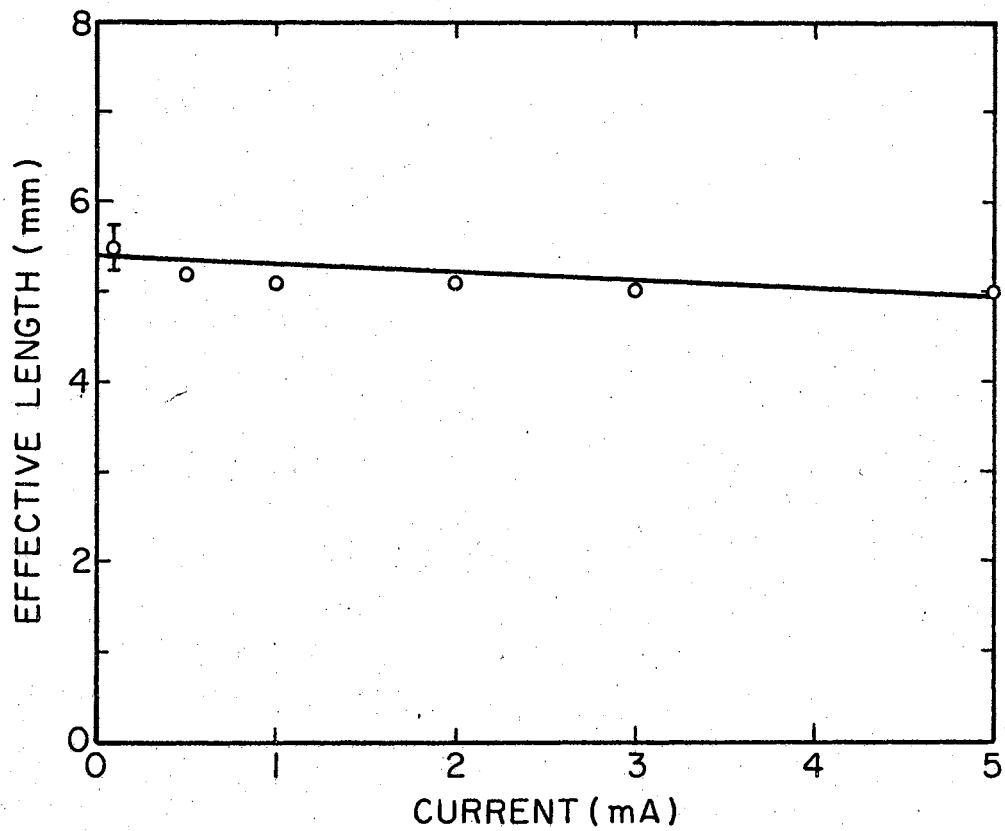

Figure 13. Effective Length of a DID - Diode 69-15

AC Behavior

The ac behavior measured is solely that of the pulse response measurements. Attempts at measurements with impedance bridges were, in comparison, very inaccurate due to severe limitations in the capabilities of available bridges. The pulse response behavior for device 69-15 is shown in Figure 14. It was this check that identified semiconductor regime operation from an ohmic or transitional behavior. Figure 14 shows the current pulse through the diode as measured by a series resistor. It is the ratio of the actual computed device

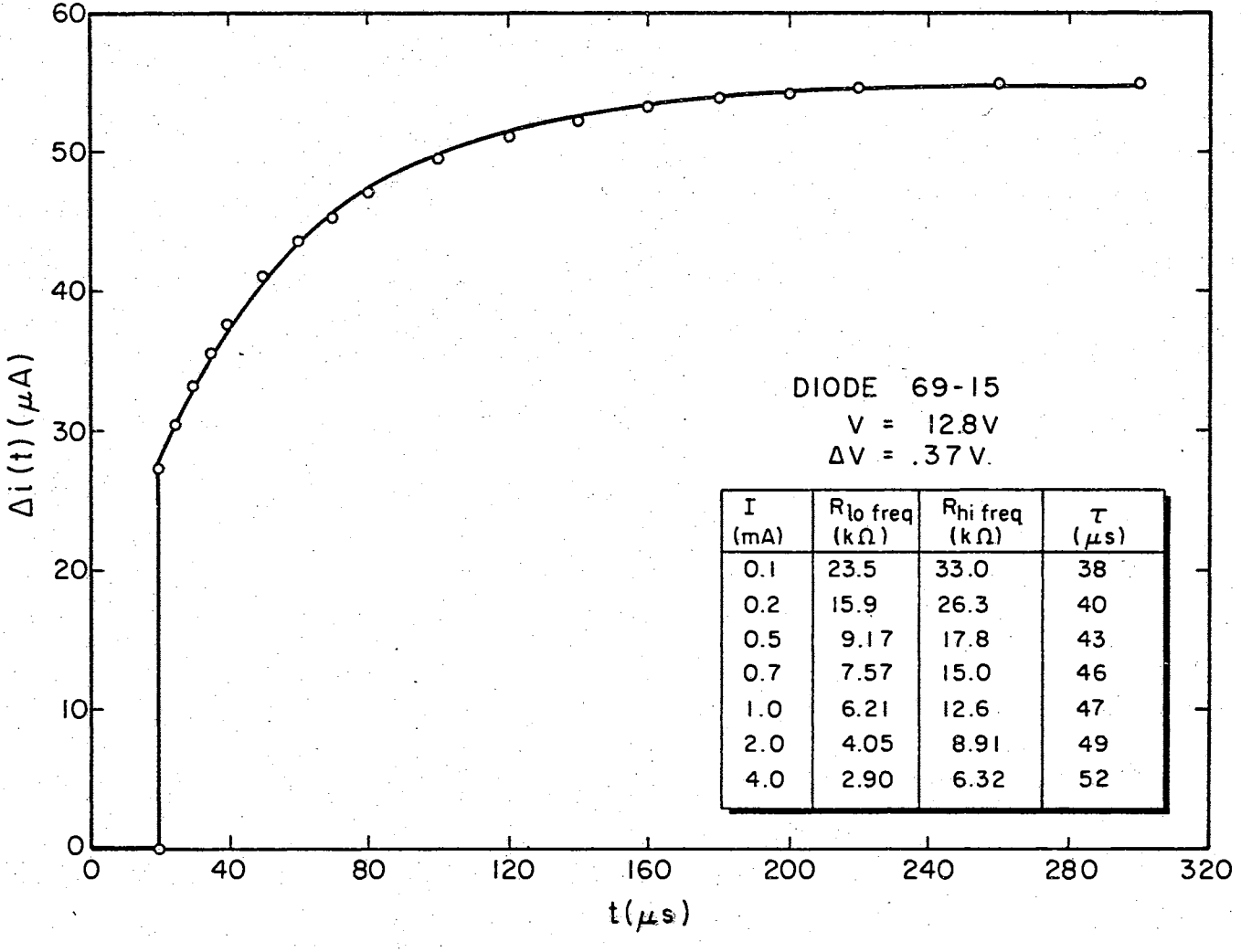

I (mA)	$R_{lo\ freq}$ (kΩ)	$R_{hi\ freq}$ (kΩ)	τ (μs)
0.1	23.5	33.0	38
0.2	15.9	26.3	40
0.5	9.17	17.8	43
0.7	7.57	15.0	46
1.0	6.21	12.6	47
2.0	4.05	8.91	49
4.0	2.90	6.32	52

Figure 14. Pulse Response - Diode 69-15

resistances, $R_{hi\ freq}/R_{lo\ freq}$ which must equal 2.0 (see Equation 2.14) for the true semiconductor regime operation. For this and other devices, the true transition point is therefore considered to be that current where the ratio 2.0 is first reached (within 5%). The table on Figure 14 shows this is achieved at a device current of 500 μA. It is somewhat difficult to state a condition for the excess carrier concentration necessary to produce semiconductor regime operation. If the excess carrier density δn is calculated from Equation 2.17 at the distance L_{eff} from the n^+-π junction (where the injected carrier density is a minimum) and it is required that $\delta n = p_T$, it would be necessary to have a device current of 2.5 mA. Thus, either the condition $\delta n = p_T$ (at the worst case position) is not a valid criterion for high level injection or the effect of this portion of the device on the overall behavior is small. As a further check on the validity of the measurements, the low frequency resistance should be related to the slope γ of the I-V characteristic by

$$R_{lo\ freq} = \frac{1}{\gamma} \frac{V_0}{I_0} \quad . \tag{4.2}$$

Agreement is within 5% in this check.

The lifetime shows a small current dependence, that is, it rises with current. This feature was generally seen in all devices, good or bad.

Noise Behavior

Noise spectra for device 69-15 operating at several different dc currents are shown in Figure 15. The basic features of g-r noise, a flat low-frequency region and a definite corner frequency followed by a

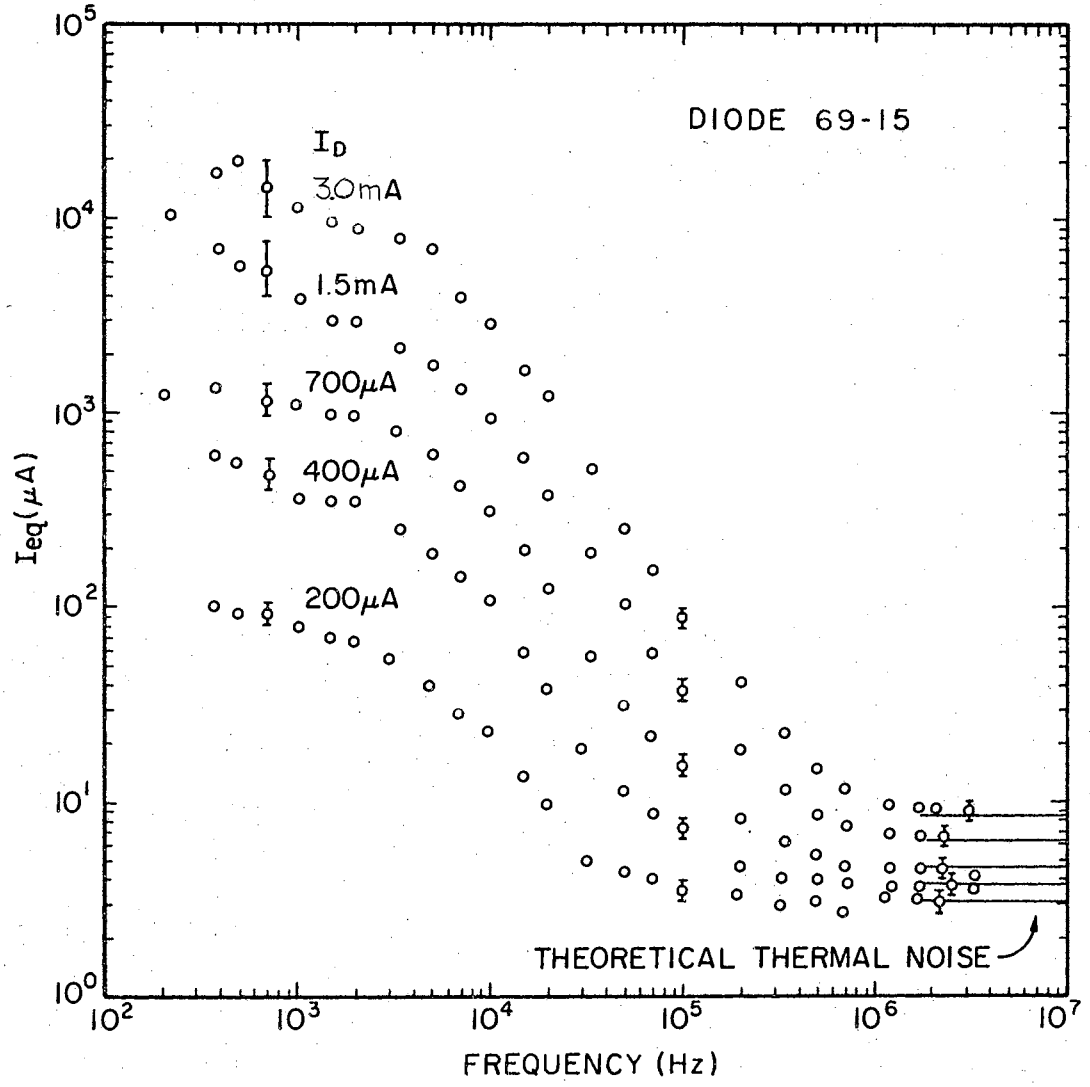

Figure 15. Noise Spectra - Diode 69-15

rapid dropoff, are distinguishable. Below the corner frequency, 1/f noise rapidly increases and this, associated with the large scattering expected of the measurement technique (see Appendix C), nearly masks the plateau. At high frequencies the noise approaches another plateau which closely matches (within 10%) the sum of the thermal noise of the amplifier input circuitry ($I_{eq\ z}$ not used in Equation 3.3) and the theoretical thermal noise of the DID at high frequency predicted by Bilger et al. (19),

$$I_{eq,th} = 2\,\frac{kT}{q}\,\frac{I}{V} \quad . \tag{4.3}$$

The actual evaluation of the low frequency plateau is done only after subtracting the thermal noise (see Figure 16) and then, by use of transparent overlays of the frequency dependencies suggested by Lee and Driedonks, the corner frequency and the I_{eq} plateau are determined. For this device, the ohmic regime g-r noise frequency factor (see Table I),

$$\zeta_1(f) = \frac{1}{1 + \omega^2\tau^2} \quad , \tag{4.4}$$

is clearly seen at low currents (up to 100 μA). At currents near the true transition point (as defined by pulse measurements) the curve is more difficult to fit and within the margin of error (see Appendix C), either the ohmic frequency factor $\zeta_1(f)$, or the semiconductor regime frequency factor developed by Driedonks,

$$\zeta_2(f) = \frac{1 + \frac{\omega^2\tau^2}{4}}{(1 + \omega^2\tau^2)(1 + \frac{\omega^2\tau^2}{16})} \quad , \tag{4.5}$$

will fit. At yet higher currents, the frequency dependence becomes more

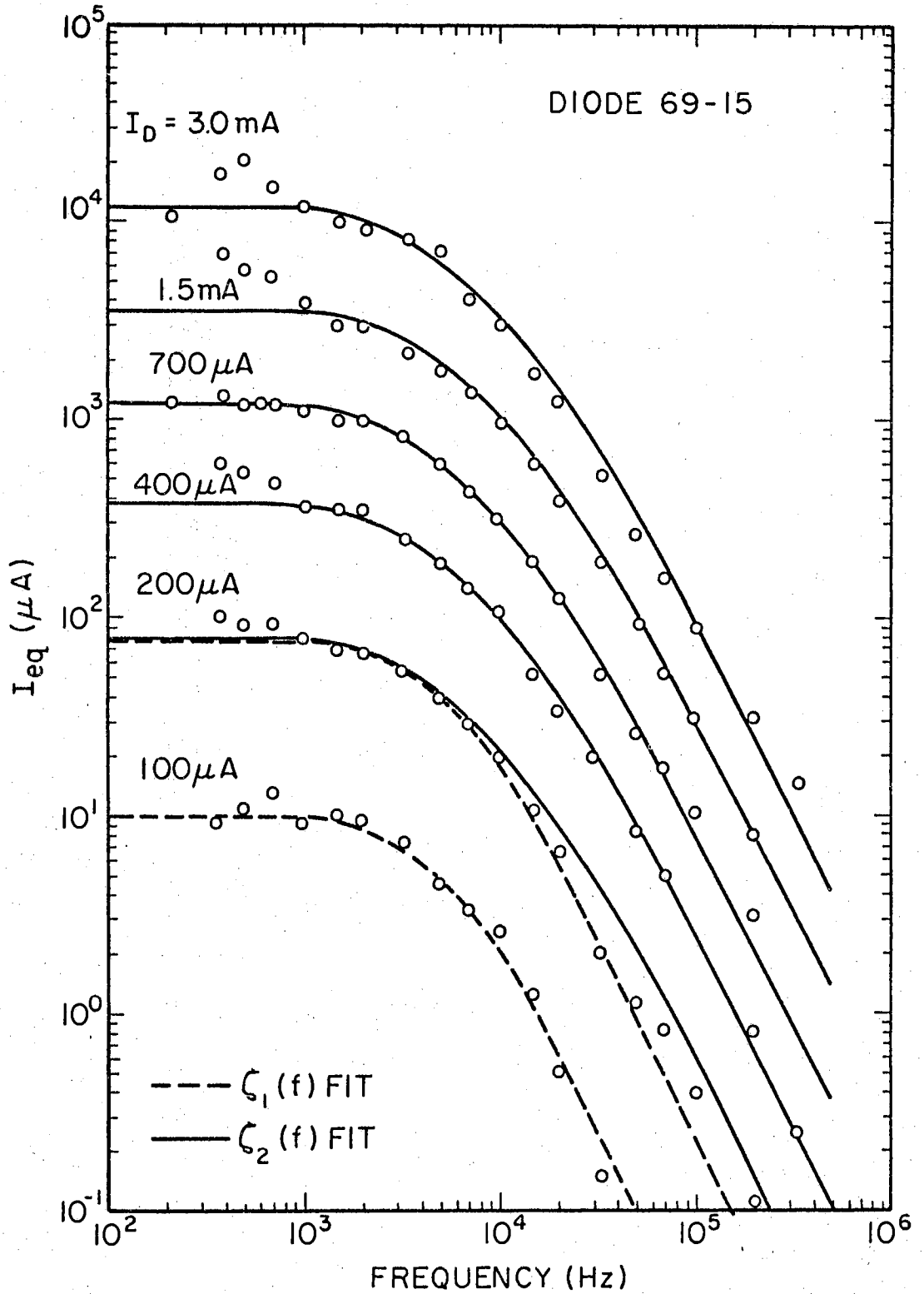

Figure 16. Adjusted Noise Spectra - Diode 69-15

and more decidedly "Driedonks" rather than the semiconductor regime frequency dependence predicted by Lee (which is the same $\zeta_1(f)$ as that expected in the ohmic regime by either theory). A frequency dependence as predicted by the Fazakas theory is not evident at all.

All three theories presented indicate the "break frequency" i.e., the corner frequency of the g-r noise spectra, is related to the lifetime by

$$\omega_c \tau = 1 \quad ,$$

where ω_c is the corner frequency in radians per second and τ is the lifetime of the injected carriers in seconds. Thus one can extract the device lifetime as well as the I_{eq} plateau in the curve fitting process. Table II shows the lifetimes extracted from both pulse and noise measurements on diode 69-15. Probable error for pulse-measurement lifetime is $\pm$ 5% and for noise-measurement lifetime is $\pm$ 20% (see Table X). Most readings agree within this error however it is significant to note that the noise measurement lifetime is systematically low. One possible explanation is that flicker noise has caused a higher apparent noise and thus a higher apparent corner frequency. There is no other evidence of flicker noise at or above the corner frequency hence this is doubtful. A second possible reason is that the correlation of noise fluctuations which lowers the noise from theoretical values somehow introduces a shift in ω_c not seen in pulse measurements.

In Figure 17, the equivalent noise current plateaus (low frequency) as determined from the curve fits are plotted for all device currents used in the noise evaluation. This plot shows the generation-recombination noise, measured in terms of an equivalent noise current,

TABLE II

LIFETIME MEASUREMENT COMPARISON - DIODE 69-15

I_D (mA)	τ_{pulse} (μs)	τ_{noise} (μs)
.1	38	33
.2	40	30
.4	—	33
.5	43	—
.7	46	40
1.0	47	36
1.5	—	43
2.0	49	40
3.0	—	38
4.0	52	—

rises rapidly from the ohmic regime predicted noise. This transitional (in terms of noise) region behavior is not clearly explainable. The noise is an order of magnitude or two above the expected ohmic regime noise. It displays the frequency response of ohmic noise and may be the result of injection high compared with the minority thermal equilibrium carrier concentration (1.5×10^{14} m^{-3} in this case) but low compared to the majority carrier concentration (1.5×10^{18} m^{-3}). At the device current of 500 μA, the noise takes on an $I_{eq} \propto I_D^{3/2}$ dependence as predicted for the transition to true semiconductor regime operation of the double-injection diode. It corresponds well with the results of the pulse response measurement which had indicated the transition was virtually completed at a device current of 500 μA (see Figure 14). Further, the magnitude of the noise is within a factor 2 of the theory as presented by Driedonks. An analysis of Equation

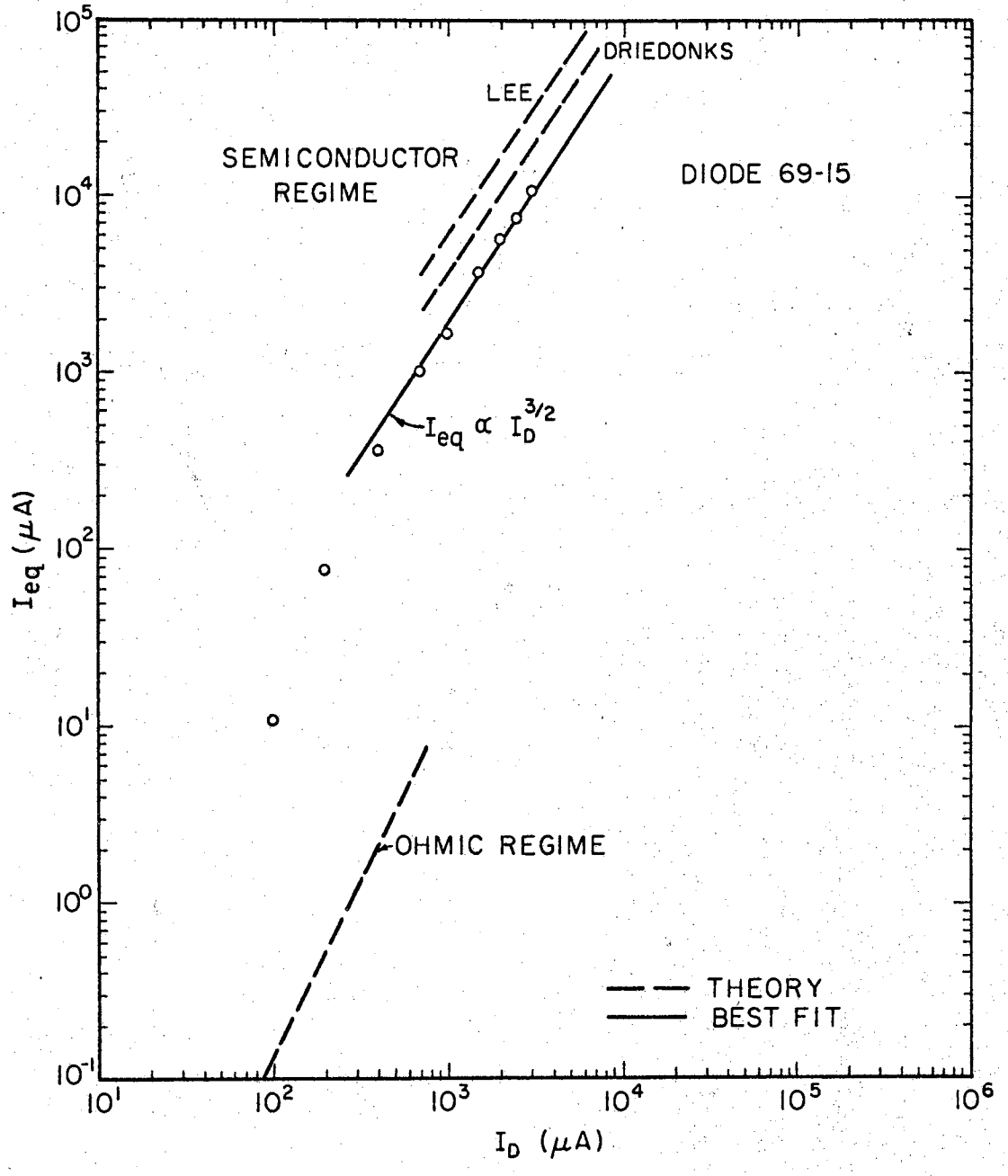

Figure 17. Noise vs Device Current - Diode 69-15

2.24[1] will show that the breakdown of the assumption $\delta n \gg p_T$ will lower the equivalent noise current only slightly. Calculations using this equation show that for regions where $\delta n = p_T$, the noise current would be .84 its original value while for $\delta n = 2p_T$, the multiplicative factor is .94, hence the effect is small indeed.

Diode 69-21

Many other double-injection diodes were constructed and evaluated in this research. Two of these devices are worthy of mention. Device 69-21 was constructed of some hyper-pure π type silicon material (Ingot B) in order to minimize any adverse effects which might be associated with traps, recombination centers or dopant atoms. The thermal equilibrium carrier density is reduced in this type material and this leads to several advantages discussed earlier.

DC Behavior

The current-voltage characteristic of device 69-21 is shown in Figure 18. Note that for this device, the dc transition to square-law behavior occurs at nearly two orders of magnitude less current than with the previous device. This corresponds to a measured resistivity of 200 kΩcm and a resultant computed thermal equilibrium carrier density of $p_T = 5.3 \times 10^{16}$ m^{-3} (and $n_T = .4 \times 10^{16}$ m^{-3}). The average effective device length, as determined from potential probe measurements, is 4.8 mm.

---

[1]Though this analysis is made using Lee's theory, the same general carrier density relationships were used by Driedonks. One then would expect the same thermal equilibrium carrier density reduction factor would result.

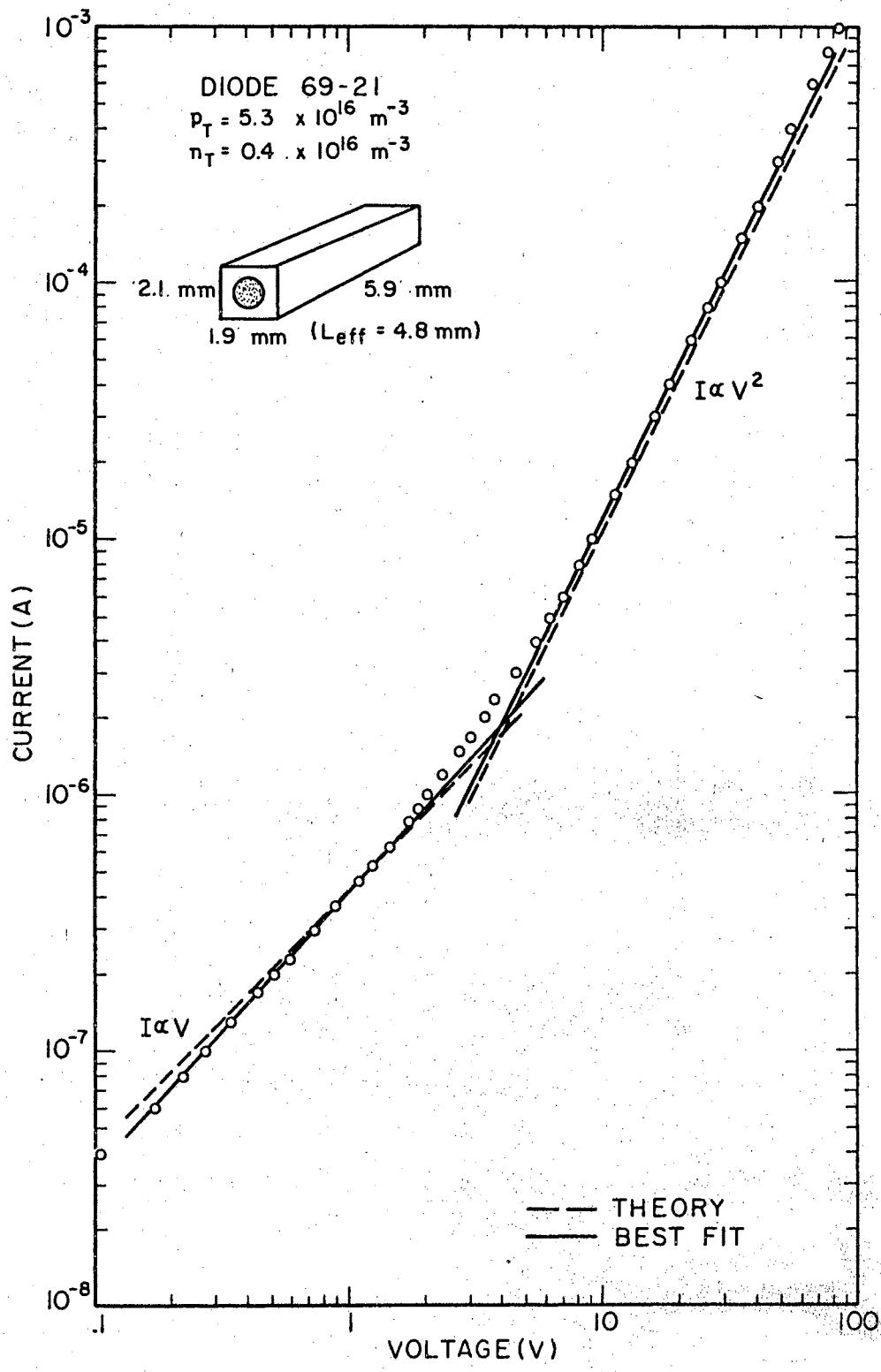

Figure 18. Current-Voltage Characteristic - Diode 69-21

AC Behavior

Pulse response data were taken as before. The results are summarized in Table III. The increase in R_{hf}/R_{lf} above 2.0 at the highest currents may be an indication of approach to insulator regime behavior (where $R_{hf}/R_{lf} = 3.0$). This, in turn, is due to the high purity of the bulk material because at this resistivity a transition to insulator regime behavior can be expected at an applied potential of 270 volts.

TABLE III

PULSE RESPONSE SUMMARY - DIODE 69-21

I_D (μA)	$R_{lo\ freq}$ (kΩ)	$R_{hi\ freq}$ (kΩ)	R_{hf}/R_{lf}	τ (μs)
5	753	1300	1.73	48
20	349	676	1.94	52
40	241	496	2.06	50
100	146	305	2.08	53
200	96	209	2.18	59
300	75	165	2.20	59

Noise Behavior

The noise spectra (Figure 19) indicate a $1/(1+\omega^2\tau^2)$ behavior indicative of a support of Lee's theory. Fazakas' theory can again be discarded on the basis of frequency dependence alone. The corner frequencies and the associated time constants (lifetimes) are discernable using the previous techniques (but with Lee's theory) and correlation

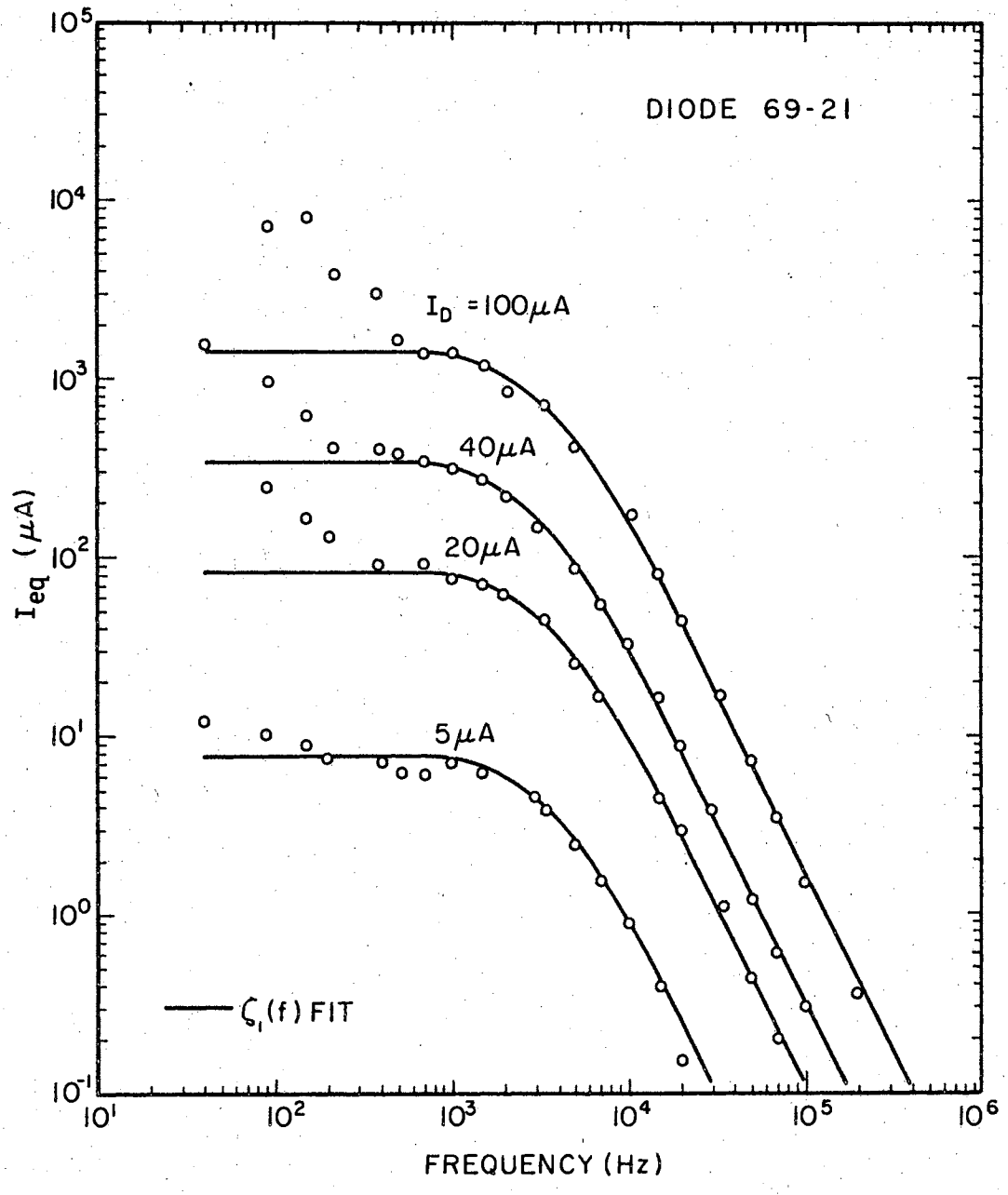

Figure 19. Noise Spectra - Diode 69-21

of these lifetimes with those determined by the pulse response method is extremely good (see Table IV). Figure 20 demonstrates the much greater theoretical noise for the ohmic regime (compare with Figure 17) and also shows the experimental data. This data does not show the steep slope transitioning to a 3/2 power slope seen in other devices but shows a less-than-theoretical ohmic noise with a transition to a slope that appears to be about 1.7. The steep low-current slope is not seen because of the much greater ohmic noise which lessens the magnitude of the transition. A possible explanation of the increased slope at higher currents is that space charge effects are becoming significant to the extent that a transition to the insulator regime has begun. This is supported by the results of the pulse response measurement. While the insulator regime g-r noise should have a more shallow ($I_{eq} \propto I_D^{4/3}$) slope, the theoretical insulator regime noise is of much greater magnitude (its value, extended to a device current of 1 mA, is 6.51×10^4 μA) and hence an increased slope similar to that experienced in the ohmic-semiconductor transition of diode 69-15 might be expected.

TABLE IV

LIFETIME MEASUREMENT COMPARISON - DIODE 69-21

I_D (μA)	τ_{pulse} (μs)	τ_{noise} (μs)
5	48	49
20	52	44
40	50	44
100	53	50
200	59	51
300	59	59

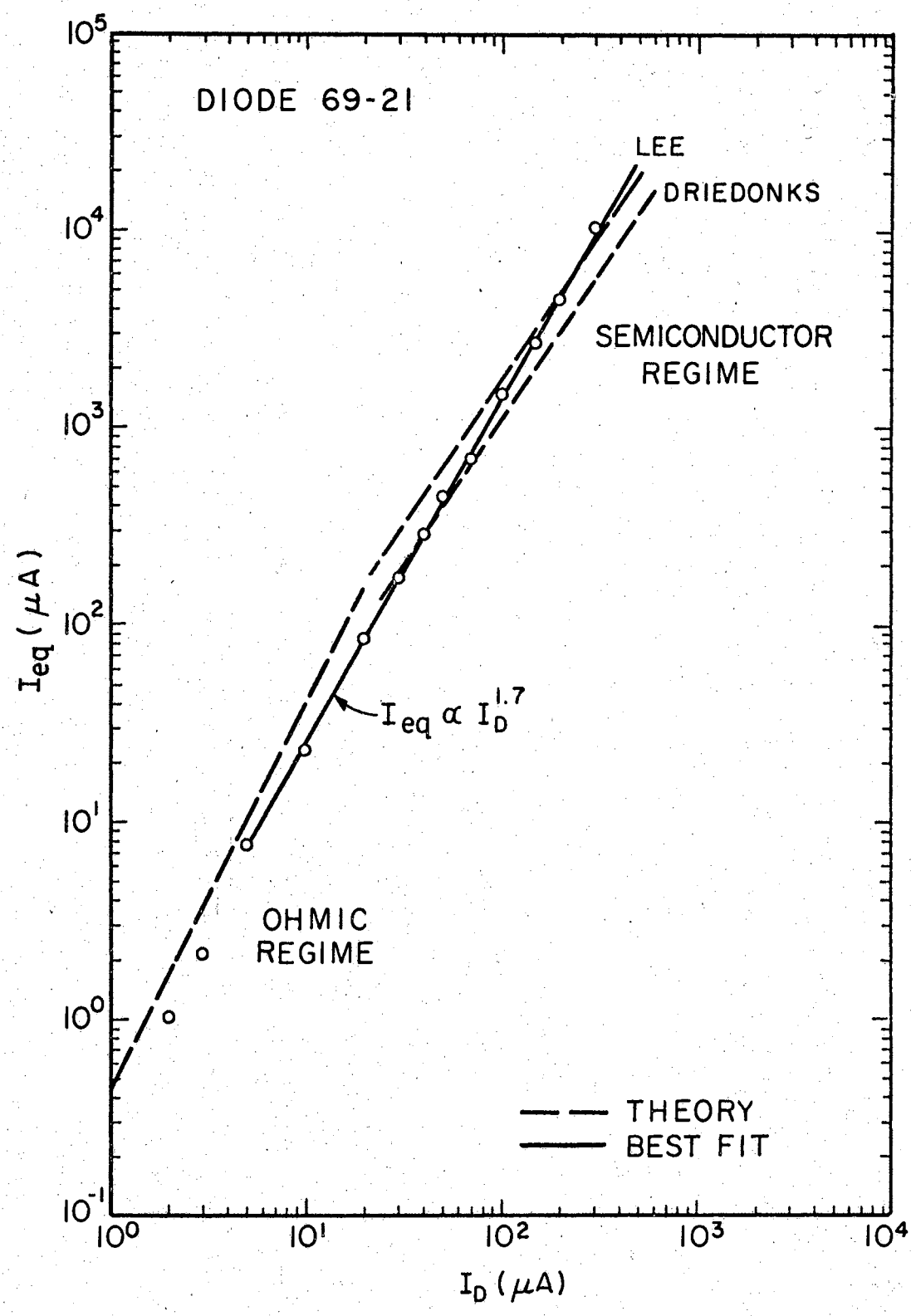

Figure 20. Noise vs Device Current - Diode 69-21

Device 69-21, then, indicates strong support for Lee's theory not only because the frequency dependence predicted by Lee, $\zeta_1(f)$, is evident but because this dependence is evident over 2 orders of magnitude of device current, a range not possible with other devices. Further, the material used for diode 69-21 is so pure that effects due to impurities are virtually eliminated.

Diode HAC-1

DC Behavior

Device HAC-1 is a double-injection diode built by the Hughes Research Laboratories and supplied to us through the California Institute of Technology. This diode has a current-voltage characteristic (see Figure 21) that is similar to that of 69-15 but with a transition (as defined by dc asymptotes) at about 50 μA. The high current slope is 2.0 as expected. At lower currents the log current-log voltage slope is 1.09. Except for the material type (π), no details were available on the parent crystal. Since the low current slope was so near the ideal 1.0, a resistivity of 74 kΩcm and a thermal equilibrium carrier density of 1.8×10^{17} m^{-3} were extracted directly from the ohmic region of the I-V plot. It should be noted that this near-ideal ohmic region slope is somewhat unexpected after experiences with other devices. A possible reason may lie in the large value of L_{eff} which may, in turn, make junction effects less preponderant. The effective length of the device was found by the potential probe method to be 6.8 mm at $I_D = 280$ μA.

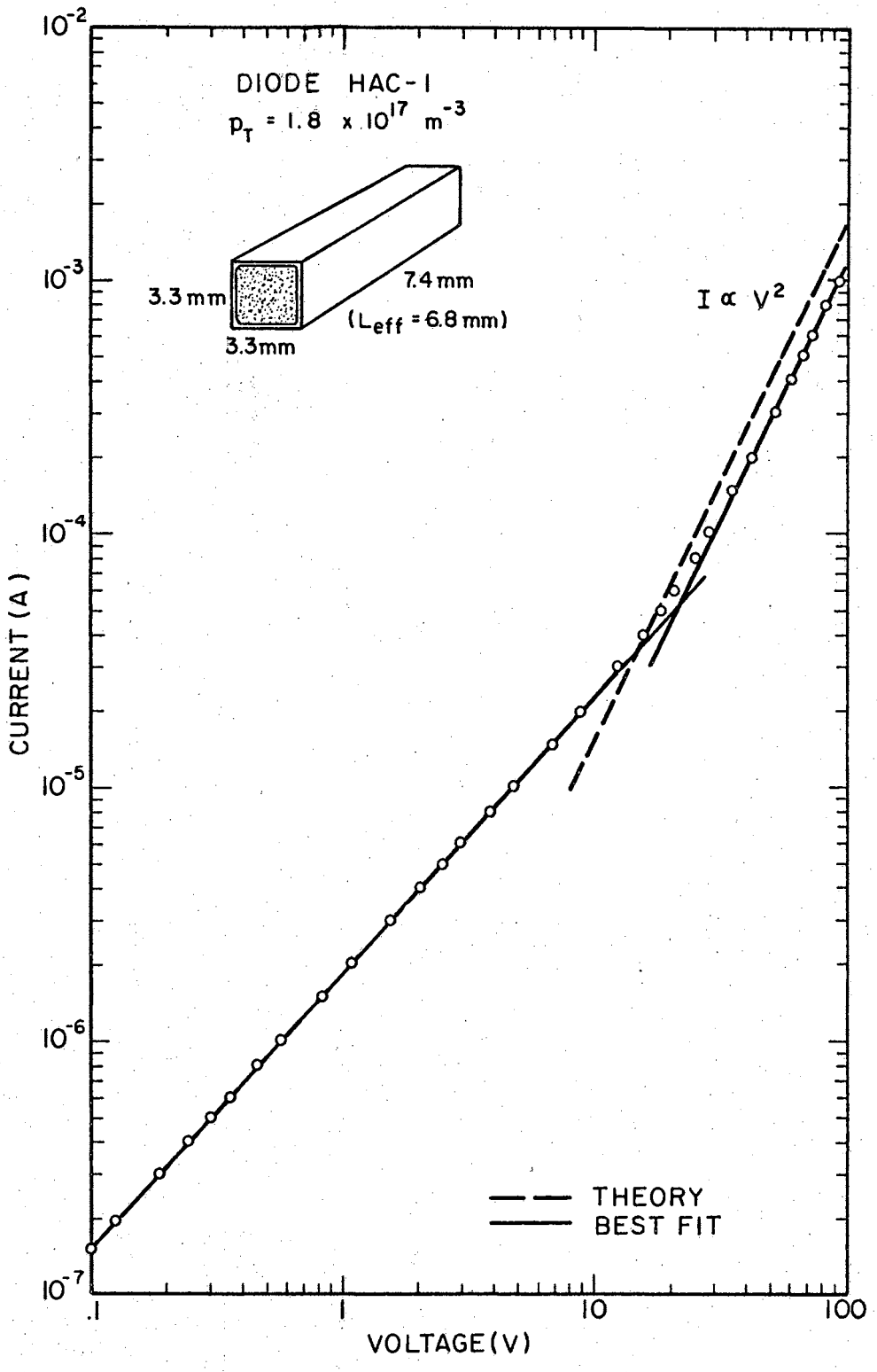

Figure 21. Current-Voltage Characteristic - Diode HAC-1

AC Behavior

The pulse response check showed the lifetime to be on the order of 20 μs. A general summary of that measurement is given in Table V. Note that this device has exhibited an extremely long transition region (slowly changing R_{hf}/R_{lf}).

TABLE V

PULSE RESPONSE SUMMARY - DIODE HAC-1

I_D (mA)	$R_{lo\ freq}$ (kΩ)	$R_{hi\ freq}$ (kΩ)	R_{hf}/R_{lf}	τ (μs)
.05	257	404	1.57	18
.1	170	302	1.78	19
.2	115	217	1.89	20
.3	91	176	1.94	21
.5	69	134	1.95	22
.65	60	117	1.95	23
.8	53	103	1.95	24
1.0	46	88.2	1.92	26
1.5	37	68.5	1.86	28

Noise Behavior

Noise spectra are illustrated in Figure 22 and again, Driedonks' theory is supported. At a current of 50 μA, the frequency dependence factor $\zeta_1(f)$ is not yet seen, evidently indicating that in this device, injection is high enough to show transitional noise behavior though the pulse behavior has not yet shown true semiconductor regime operation

The plot of I_{eq} vs I_D (Figure 23) again shows the measured noise

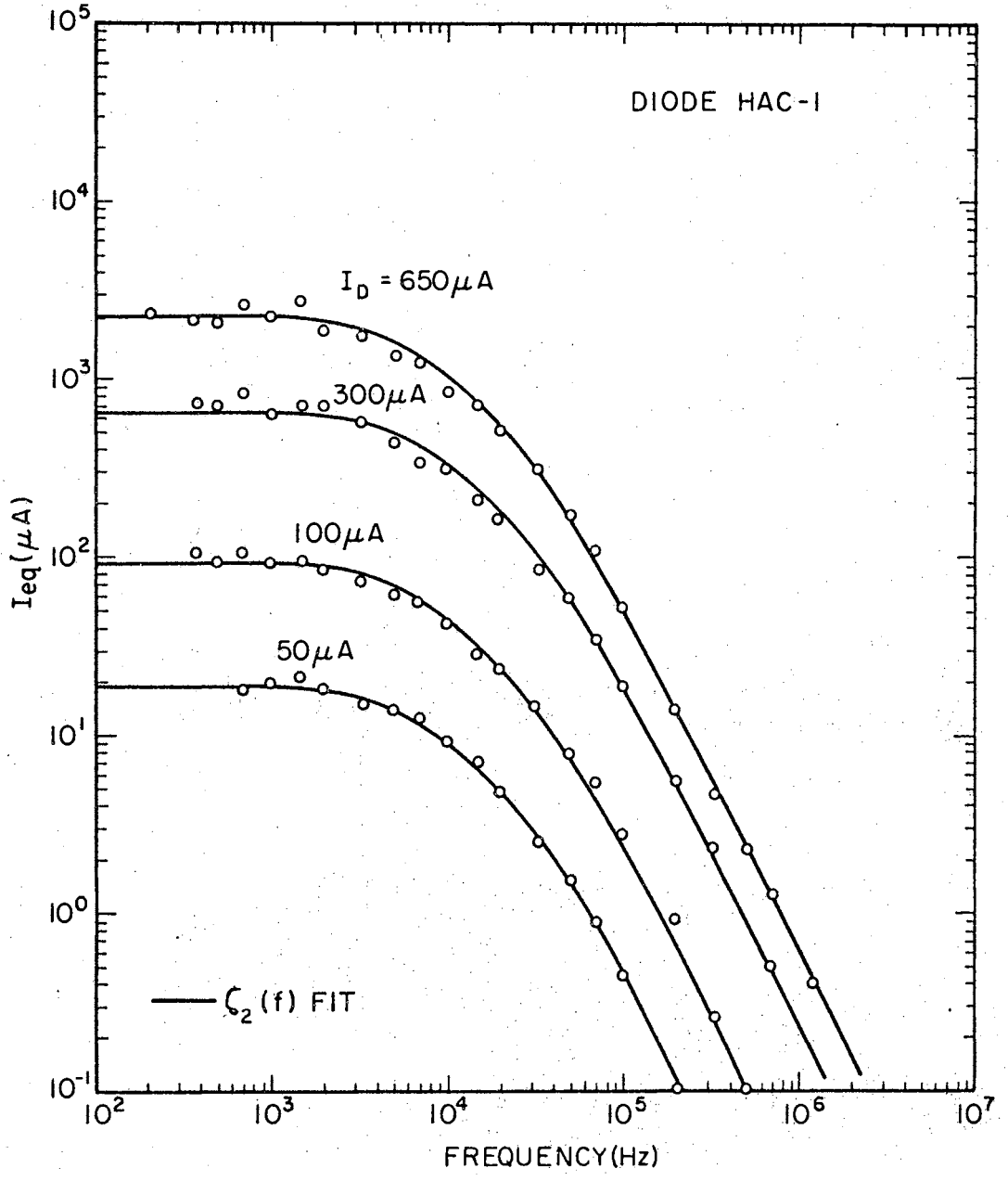

Figure 22. Noise Spectra - Diode HAC-1

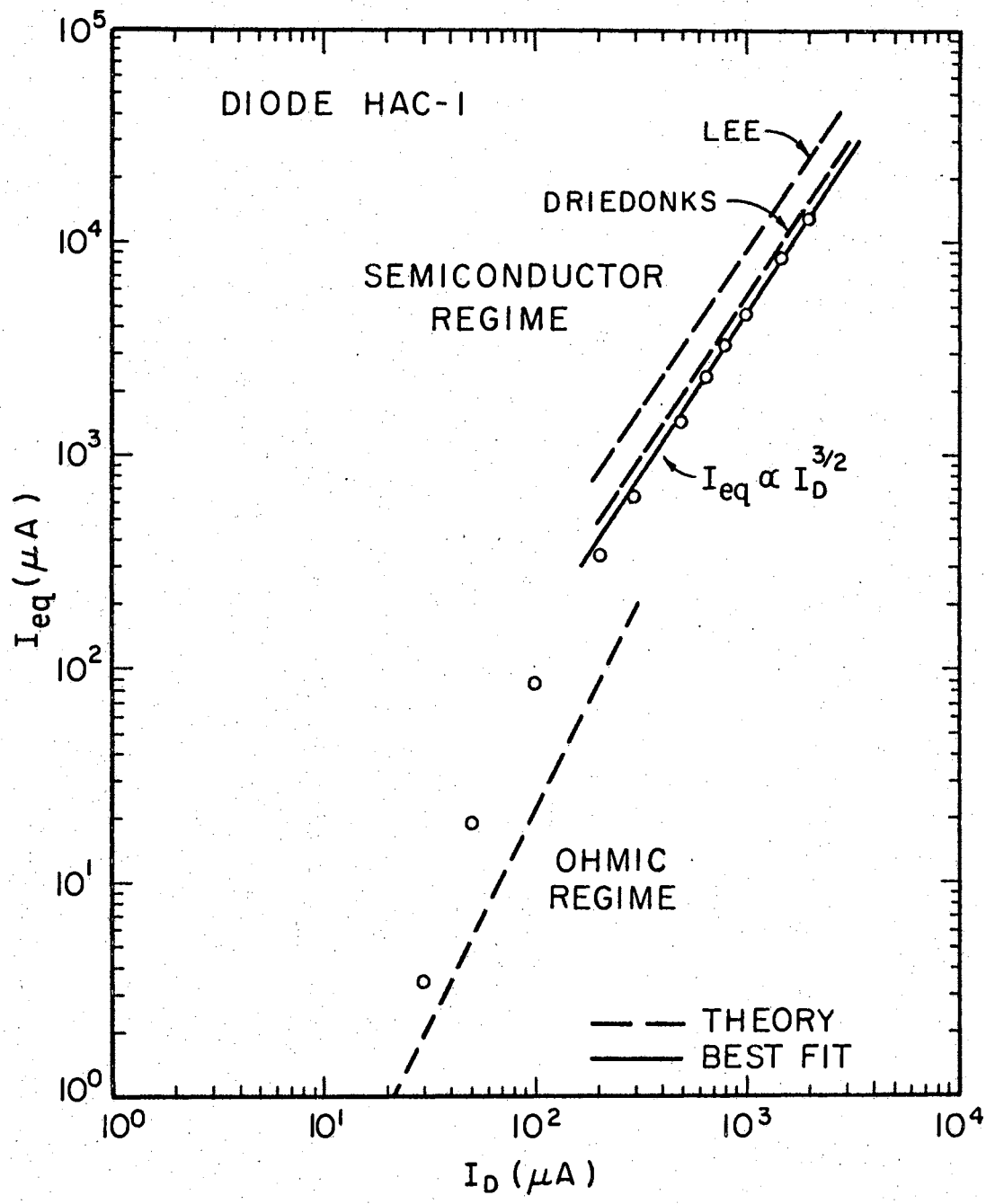

Figure 23. Noise vs Device Current - Diode HAC-1

to be somewhat less than the predicted value but the difference is now well within the errors of measurement. A comparison of the lifetimes taken from pulse response and noise (Driedonks' factor) again shows good agreement (see Table VI).

TABLE VI

LIFETIME MEASUREMENT COMPARISON - DIODE HAC-1

I_D (mA)	τ_{pulse} (μs)	τ_{noise} (μs)
.1	19	20
.2	20	20
.3	21	18
.5	22	18
.65	23	22
.8	24	20
1.0	26	22
1.5	28	26

This device, then, is in material and in behavior "between" the diodes 69-15 and 69-21. It shows semiconductor regime behavior according to Driedonks' theory and the current dependence of the noise seems to indicate a long slow transition to an $I_{eq} \propto I_D^{3/2}$ behavior.

Summary

A summary of the behavior of the three devices reported on is included as Table VII. It should be noted that the bulk material used varies in resistivity over more than an order of magnitude. Processes

TABLE VII

DEVICE SUMMARY

	69-15	69-21	HAC-1
$\rho(k\Omega m)$	8.7×10^{-2}	2.0×10^{0}	7.4×10^{-1}
p_T (m^{-3})	1.5×10^{18}	5.3×10^{16}	1.8×10^{17}
n_T (m^{-3})		$.4 \times 10^{16}$	
A (m^2)	9.0×10^{-6}	4.1×10^{-6}	1.09×10^{-5}
L (m)	6.0×10^{-3}	5.9×10^{-3}	7.4×10^{-3}
L_{eff} (m)	5.1×10^{-3}	4.8×10^{-3}	6.8×10^{-3}
Theoretical			
DC Transition to Semiconductor Regime (μA)	77.5	1.55	36.0
DC Transition to Insulator Regime (μA)	5.41×10^{8}	7.61×10^{3}	6.51×10^{5}
Experimental			
DC Transition to Semiconductor Regime (μA)	180	1.9	52
AC Transition to Semiconductor Regime (μA)	500	20	~ 250
Noise Transition to Semiconductor Regime (μA)	500	not clear	not clear
$< \tau_{pulse} >$ (μs)	45	53	23
$< \tau_{noise} >$ (μs)	37	49	21

used in their construction are essentially the same. Devices 69-15 and HAC-1 seem to support Driedonks' theory yet device 69-21, the "cleanest" of all the devices, shows a support of Lee's theory. A large variation in the magnitude of the 1/f noise does exist. It may thus be worthwhile to pursue reduction of this noise in order that still more decisive g-r noise experiments might be conducted.

CHAPTER V

CONCLUSIONS AND RECOMMENDATIONS

Summary and Conclusions

An outline of the dc and ac theory of operation of a double-injection diode has been given and a summarizing account of three different noise theories has been presented.

An interesting feature of the noise theory is that the equivalent noise current is always related to the carrier density and electric field by:

$$I_{eq} \propto n\, E^2 \quad ,$$

and it turns out that the noise can thus be surmised from the relations,

Ohmic Reg.	: $n = \text{const.}$, $I \propto E$	so	$I_{eq} \propto I^2$
Semicond. Reg.	: $n \propto I^{\frac{1}{2}}$, $I \propto E^2$	so	$I_{eq} \propto I^{3/2}$
Insulator Reg.	: $n \cdot E \propto I$, $I \propto E^3$	so	$I_{eq} \propto I^{4/3}$.

Devices were constructed so as to optimize the existence and appearance of the semiconductor regime, where injected carrier densities are high compared to thermal equilibrium carrier densities. The dc and ac measurements of the device behaviors indicated an acceptable method of double-injection diode construction had been developed such that reliability and reproducibility were optimized.

The total noise of each device was measured and the known thermal

noise was subtracted. Curve fit techniques were then used to analyze the generation-recombination noise (which remained) for the diode in both the ohmic (low currents) and semiconductor (high currents) regimes. For the semiconductor regime, the three available theories differ only by a constant in their determination of the magnitude of the noise at low frequencies (a plateau). Because of the approximations made and the errors of the measurements, it is not possible to discern between theories on this basis. The current dependence of the three theories is also identical hence again no discrimination is possible. The frequency dependencies of the three theories applied to the semiconductor regime of DID operation are quite different however, being as follows:

$$\zeta_1(f) = \frac{1}{1+\omega^2\tau^2} \qquad \text{(Lee)}$$

$$\zeta_2(f) = \frac{1 + \frac{\omega^2\tau^2}{4}}{(1+\omega^2\tau^2)(1 + \frac{\omega^2\tau^2}{16})} \qquad \text{(Driedonks)}$$

$$\zeta_3(f) = \frac{1}{\omega^{3/2}} \text{ with bumps} \qquad \text{(Fazakas)} \quad .$$

Fazakas' theory was discarded early in the research since none of the many devices constructed indicated anything near the complex frequency dependence (or even its envelope) predicted. It was somewhat more difficult to determine whether Lee's theory or Driedonks' theory was a better approximation to the true situation.

Devices 69-15 and HAC-1 clearly demonstrated the frequency dependence predicted by Driedonks. On the other hand, device 69-21 follows Lee's predictions and its higher purity bulk material would normally be

thought to produce the more credible data. Two explanations for the difference are possible. The dc transition from the ohmic to the semiconductor regime is not a function of the purity of the material (except indirectly through the lifetime). The dc transition from the semiconductor regime to the insulator regime is proportional to the thermal equilibrium carrier concentration. Thus for device 69-21, the separation between the ohmic and insulator regimes is less than two orders of magnitude of applied voltage. Device 69-21 may have exhibited a transitional (noise-wise) behavior over its entire range of operation such that the frequency factor $\zeta_1(f)$ predicted by either theory for the ohmic and insulator regimes dominated throughout its operation. An alternative explanation is that neither theory can predict the magnitude of the g-r noise for the full range of bulk material characteristics. Driedonks claims the basic difference in the two approaches is the treatment of the correlation of noise fluctuations in adjacent cross sections of the diode. It could be that his inclusion of this correlation does apply to the more extrinsic cases of devices 69-15 and HAC-1 but not to the virtually intrinsic case of 69-21. In this event a more detailed study of noise correlations in semiconductor materials is necessary. It may also be that ambipolar drift effects introduce modifications to the frequency dependence. A discussion of such effects, mentioned only briefly by van der Ziel (1), is beyond the scope of this study, however the general result is to introduce "oscillations" in the noise spectra. The absence of these oscillations makes this condition doubtful.

In summary, this research has produced several important results. First, generation-recombination noise has been shown to exist in a

double-injection diode operating in the "ohmic" regime and in the "semiconductor" regime. Secondly, there is no question that this g-r noise does eventually take on an ω^{-2} frequency dependence. This result rules out Fazakas' theory and indicates the behavior of the generation-recombination process under high-level injection conditions is similar (statistically, at least) to that in a semiconductor crystal without injection. Thirdly, the time constant τ evaluated from the noise corner frequency is numerically quite close to the lifetime of excess carriers evaluated by the pulse response technique. Further, the magnitude of the low frequency g-r noise plateau is essentially that given by Driedonks' theory or by Lee's theory (difference of factor 3/2) under the modified admittance definition (see Equation 2.22). Lee's original definition of the differential slice resistance (see footnote 2, page 15) is shown to be wrong (the g-r noise then being 4 times larger than under his modified definition). Finally, the frequency dependencies near the corner frequencies support Driedonks' theory in two cases and Lee's theory in the other case. It may be that in the latter case the effects of the operating proximity to the insulator regime caused a transitional behavior to predominate over the entire range of operation. Alternatively, it may be that neither the treatment by Lee nor that by Driedonks fully accounts for the range of available dopant concentrations or for the correlation of fluctuations in adjacent portions of the semiconductor diode.

Recommendations for Further Study

It would be extremely interesting to study the generation-recombination noise of double-injection diodes made by the

ion-implantation method. Little work has been done in the noise aspects of these relatively new diodes and their more clean and uniform junction nature may provide cleaner spectra and otherwise more interesting results.

An investigation into the effects of temperature and applied magnetic field on generation-recombination noise would be quite informative and may even provide a key to noise correlation effects in such materials. This type study has been performed on some types of semiconductor noises but not, to the author's knowledge, to generation-recombination noise (some temperature effects on g-r noise in crystals have been studied). Noise measurement techniques may be difficult to develop for these cases.

BIBLIOGRAPHY

(1) van der Ziel, A. Fluctuation Phenomena in Semi-conductors. London: Butterworths Scientific Publications, 1959.

(2) van der Ziel, A. Noise. New York: Prentice-Hall, 1954.

(3) Bennett, W. R. Electrical Noise. New York: McGraw-Hill, 1960.

(4) King, R. A. Electrical Noise. London: Chapman and Hall, 1966.

(5) MacDonald, D. K. C. Noise and Fluctuations: An Introduction. New York: Wiley, 1962.

(6) Nyquist, H. "Thermal Agitation of Electric Charge in Conductors." Physical Review, Vol. 32 (1928), 110.

(7) Johnson, J. B. "Thermal Agitation of Electricity in Conductors." Physical Review, Vol. 32 (1928), 97.

(8) Williams, N. H. and E. W. Thatcher. "On Thermal Electronic Agitation in Conductors." Physical Review, Vol. 40 (1932), 121.

(9) Bernamont, J. "Fluctuations de Potentiel aux Bornes d'un Conductor Metallique de faible Volume parcouru par un Courant." Annales de Physique, Vol. 7 (1937), 71.

(10) Herzog, G. B. and A. van der Ziel. "Shot Noise in Germanium Single Crystals." Physical Review, Vol. 84 (1951), 1249.

(11) Hill, J. E. and K. M. Van Vliet. "Generation Recombination Noise in Intrinsic and Near-Intrinsic Germanium Crystals." Journal of Applied Physics, Vol. 29 (1958), 177.

(12) McCarter, E. R. "A Reversible Nuclear Radiation Approach to Generation-Recombination Noise Studies in Ge-Single Crystals." (unpub. Ph.D. dissertation, Oklahoma State University, 1967).

(13) Yau, L. D. and C. T. Sah. "Theory and Experiments of Low-Frequency Generation-Recombination Noise in MOS Transistors." IEEE Transactions on Electron Devices, Vol. ED-16 (1969), 170.

(14) Lampert, M. A. and A. Rose. "Volume-Controlled, Two Carrier Currents in Solids: The Injected Plasma Case." Physical Review, Vol. 121 (1961), 26.

(15) Baron, R. "Effects of Diffusion on Double Injection in Insulators." Physical Review, Vol. 137 (1964), A272.

(16) Mayer, J. W., R. Baron, and O. J. Marsh. "Observation of Double Injection in Long Silicon p-i-n Structures." Physical Review, Vol. 137 (1965), A286.

(17) Baron, R. "Effects of Diffusion and Thermal Generation on Double Injection in Semiconductors." Journal of Applied Physics, Vol. 39 (1968), 1435.

(18) Mayer, J. W., O. J. Marsh, and R. Baron. "Double Injection in Long Silicon p-π-n Structures." Journal of Applied Physics, Vol. 39 (1968), 1447.

(19) Bilger, H. R., D. H. Lee, M-A. Nicolet, and E. R. McCarter. "Noise and Equivalent Circuit of Double Injection." Journal of Applied Physics, Vol. 39 (1968), 5913.

(20) Driedonks, F., R. J. J. Zijlstra. "Double Injection and Noise in Germanium Diodes." Proceedings of the Conference on Physical Aspects of Noise in Electronic Devices, Nottingham, 1968.

(21) Baron, R. and J. W. Mayer. "Double Injection in Semiconductors." (to be published in Semiconductors and Semimetals, edited by R. K. Willardson and A. C. Beer).

(22) Lee, Louis L. S. "Generation Recombination Noise Spectra of a Double-Injection Diode." (unpub. Ph.D. dissertation, Oklahoma State University, 1969).

(23) Lee, D. H. "Double Injection: High Frequency Noise and Temperature Dependence." (unpub. Ph.D. dissertation, California Institute of Technology, 1969).

(24) Van Vliet, K. M. "On the Equivalence of the Fokker-Planck Method and the Free-Energy Method for the Calculation of Carrier Density Fluctuations in Semiconductors." Physica, Vol. 23 (1957), 248.

(25) Burgess, R. E. "Fluctuations in the Number of Charge Carriers in a Semiconductor." Physica, Vol. 20 (1954), 1007.

(26) Burgess, R. E. "Fluctuations of the Number of Electrons and Holes in a Semiconductor." Proc. Phys. Society, London, Vol. B68 (1955), 661.

(27) Shockley, W. and W. T. Read, Jr. "Statistics of the Recombinations of Holes and Electrons." Physical Review, Vol. 87 (1952), 835.

(28) Bilger, H. R., P. R. Worch, L. L. Lee, and M-A. Nicolet. "Generation-Recombination Noise in Double-Injection Diodes." Solid State Electronics, Vol. 12 (1969), 849.

(29) Langevin, M. P. "Sur la Théorie du Mouvement Browniens." Compters Rend. Acad. Sci., Paris, Vol. 146 (1908), 530.

(30) Driedonks, F., private communication (to be published as Ph.D. dissertation and in Physica), 1969.

(31) Fazakas, A. B. and A. Friedman. "On the Double Injection Current Noise in Solids." Phys. Stat. Sol., Vol. 28 (1968), 385.

(32) Sergiescu, V., private communication with M-A. Nicolet, 1969.

(33) Worch, P. R., L. S. Lee, and H. R. Bilger. "Fluctuation Phenomena in Silicon Double Injection Diodes." 1969 SWIEECO Record. New York: IEEE (1969).

(34) Bendat, J. S. and A. G. Piersol. Measurement and Analysis of Random Data. New York: Wiley, 1958.

APPENDIX A

LIST OF SYMBOLS

A	Cross sectional area		(m^2)
α	Relative standard error		
b	Mobility ratio	$(\mu_n/\mu_p=2.81)$	
β	kT/q	(.026)	(V)
γ	Slope of log current-log voltage characteristic		
δn	Injected electron concentration		(m^{-3})
δp	Injected hole concentration		(m^{-3})
E	Electric field strength		$(V \cdot m^{-1})$
E_0	DC electric field strength component		$(V \cdot m^{-1})$
$\tilde{e}$	Sinusoidal electric field strength component		$(V \cdot m^{-1})$
$\varepsilon\varepsilon_0$	Dielectric constant	$(12x8.85x10^{-12})$	$(A \cdot s \cdot V^{-1} \cdot m^{-1})$
f	Frequency		(Hz)
I	Current		(A)
$\overline{I^2}$	Variance of current fluctuations		(A^2)
I_0	DC current		(A)
I_c	Noise calibrator diode current		(A)
I_D	Device current		(A)
I_{eq}	Equivalent shot noise diode current		(A)
$I_{eq\ z}$	Equivalent noise current of amplifier input circuitry		(A)
i	Instantaneous current value		(A)
$\tilde{i}$	Sinusoidal component of current		(A)

J	Total current density		$(A \cdot m^{-2})$
J_n	Electron current density		$(A \cdot m^{-2})$
J_p	Hole current density		$(A \cdot m^{-2})$
J_0	DC current density component		$(A \cdot m^{-2})$
$\tilde{j}$	Sinusoidal current density component		$(A \cdot m^{-2})$
k	Boltzmann's constant	(1.38×10^{-23})	$(joule \cdot {}^{o}K^{-1})$
L	Device length (near-intrinsic region)		(m)
L_a	Ambipolar diffusion length		(m)
L_{eff}	Effective device length (near-intrinsic region)		(m)
μ_n	Electron mobility	$(.135)$	$(m^2 \cdot V^{-1} \cdot s^{-1})$
μ_p	Hole mobility	$(.048)$	$(m^2 \cdot V^{-1} \cdot s^{-1})$
N	Total number of electrons		
N_T	Number of electrons at thermal equilibrium		
n_T	Equilibrium electron concentration		(m^{-3})
n	Electron concentration		(m^{-3})
n_i	Intrinsic carrier concentration	$(n_i^2 = n_T p_T)$	(m^{-3})
n^+	Heavily n material or region	$(n_T \gg p_T)$	
ν	Slightly n material	$(n_T > p_T)$	
P	Total number of holes		
P_T	Number of holes at thermal equilibrium		
p	Hole concentration		(m^{-3})
p_T	Equilibrium hole concentration		(m^{-3})
p^+	Heavily p material or region	$(p_T \gg n_T)$	
π	Slightly p material	$(p_T > n_T)$	
q	Electron charge	(1.6×10^{-19})	$(A \cdot s)$
R	Resistance		(Ω)
r	Net recombination rate		$(m^{-3} s^{-1})$

ρ	Resistivity		(Ωm)
S_i	Spectral density (current)		($A^2 \cdot s$)
S_v	Spectral density (voltage)		($V^2 \cdot s$)
T	Temperature	(300)	(^oK)
t	Time		(s)
τ	Carrier (Shockley-Read) lifetime		(s)
V	Voltage		(V)
$\overline{V^2}$	Variance of voltage fluctuations		(V^2)
V_0	DC component of applied voltage		(V)
$\tilde{v}$	Sinusoidal component of applied voltage		(V)
ω	Angular frequency		($rad \cdot s^{-1}$)
x	Distance along longitudinal axis of device		(m)
Y	Admittance		(Ω^{-1})
ψ	Potential		(V)
ζ	Frequency dependence factor		

APPENDIX B

DEVICE PREPARATION

Some of the double-injection diodes used in the research for this dissertation and the associated papers (28,33) were prepared by the author during two trips to the California Institute of Technology where he worked under the guidance of Dr. M-A. Nicolet, Professor of Electrical Engineering there. Other diodes were made at this institution. Minor variations in procedures are inevitable but this appendix does include the essential steps in the fabrication of silicon double-injection diodes using either ν or π material and using aluminum for p^+ junctions and lithium for the n^+ junctions.

Materials

The material used for the devices of this study (except HAC-1) was from one of two ingots with initial specifications as appear in Table VIII.

Slicing and Rough Cutting

A Felker Model 80B0 saw with a .015" thick diamond blade was used to slice the ingot which had been mounted on a glass plate with melted "black wax". A water-oil mixture sprayed on both sides of the blade kept the blade cool and carried the particles away. Graduated increments of .001" on the two orthogonal carriage adjustments provided

TABLE VIII

MATERIAL SPECIFICATIONS

Ingot "A"	
Mfr.:	Alleghany Electric Chemicals Co. Bradford, Pennsylvania
Identification No.:	57873-2
Material:	Silicon, Single Crystal, Float Zone
Type:	P 1-1-1
Dopant:	Boron
Resistivity:	8700 Ωcm
Diameter:	2.35 cm
Length:	5.0 cm
Weight:	34.0 gm
Dislocations:	NS
Lifetime:	NS

Ingot "B"	
Mfr.:	Wacker Chemicals Corp. Munich, Germany
Identification No.:	20041-3
Material:	Silicon, Single Crystal, Float Zone
Type:	P 1-1-1
Dopant:	Boron
Resistivity:	200 kΩcm, measured
Diameter:	2.47 cm
Length:	7.0 cm
Weight:	79.8 gm
Dislocations:	NS
Lifetime:	3000 μs, minimum

precise adjustment of the slice thickness. A dashpot-type arrangement allowed slow and even application of vertical pressure to the blade. After the slices were cut, the brass/glass mounting plate was heated and the slices removed. Some devices were then sliced to shape while

others of more irregular shapes were diced with a Raytheon Model 2-334 100 watt ultrasonic impact grinder. The die, resembling in shape and function a cookie cutter, was mounted in the ultrasonic (22-28 kHz) transducer head, and with a force of 1 to 1.5 lbs., lowered to the silicon chip. In this case a melted brown wax, also called "sticky wax", was used to mount the chip to a microscope slide piece which was then mounted on a cylindrical base placed in the grinder.

Of great importance, and actually the key to the grinding action is the slurry compound. It was this mixture of abrasive compound and water which actually performed the grinding. Buehler No. 40-6460AB 400 mesh grinding compound was used, mixed 1:1 by volume with water. The mixture was sprayed directly on the silicon where the die came in contact with it and precautions were taken to prevent settling-out of the grinding compound by arrangement of hoses and agitation at the cutting point. While maintaining system resonance and constant pressure were important, proper handling of the slurry compound had the most pronounced effect on cutting speed. When it occurred that the cutting action slowed or stopped it was invariably the slurry compound flow which was at fault. Clogged lines, loss of compound and lack of agitation were primarily to blame.

Removal of the shape from the die, while initially appearing difficult, was quite easily accomplished simply by immersing the resonating grinding head in a beaker of water. With a slight re-tuning, the resonating die quickly discharged the silicon shape.

Lapping

Devices were lapped using a glass plate and a slurry of grinding compound. Grit sizes of 400, 800, 1200 and 3200 mesh were used in turn to assure a smooth surface. Special precautions were taken to preclude transferring larger grit compound to the next finer lapping operation and the device was carefully inspected for uniformity between each lapping stage. No scratches or rough spots which might have caused preferential etching were allowed.

Pre-etch Cleaning

The silicon block was placed in a beaker with about 25 cc of trichloroethylene and cleaned for two minutes in the ultrasonic cleaner. The block was then swished around in about 25 cc of acetone for one minute and left in the acetone until preparations for the next step were completed. From this point on until the device was clamped for placement in the vacuum unit, it was kept covered with the appropriate liquid at all times. About 40 cc of nitric acid (70% - reagent grade) was placed in a beaker over a Bunsen burner. The greatest portion of the acetone was poured off and the device slipped into the nitric acid. The beaker was heated for about 10 minutes until the acid became a dark yellow in color or until the beaker became so hot it could not be held in the fingers for more than 2-3 seconds. The device was then flushed several times with nitric acid and left in the acid pending the next phase.

Etch

A mixture of 20 ppv nitric acid to 1 ppv hydrofluoric acid (48%) (about 20 cc total) was prepared of which about 10 cc was placed in a plastic beaker and the device, with nearly all nitric acid drained from the beaker, slipped in. The etching action became immediately evident from the yellowing of the solution. The etching process takes about 30 minutes during which the bath was continuously agitated to prevent air bubbles from affecting the etch. The device was turned over at least once to assure the other side was properly etched. When the etchant became mildly yellow, it was flushed out with fresh etchant. The etch was considered completed when the entire surface was uniformly very shiny. The etch rate for silicon is about 1 mil per 20 minutes. The etch was quenched with methanol and the device left therein.

Evaporation

The evaporation of the aluminum p^+ contact was accomplished by electrically heating a specially-prepared tungsten filament about which was wrapped the material to be evaporated. The evaporation was done in a Veeco Model VE-400 high vacuum deposition system. The tungsten filament was .030 - .040" wire with a small dip near the center about which fine tungsten wire was wrapped at the point where the melt was to form to help prevent dripping of the aluminum.

For each aluminum contact, 20-40 mm of .032" diameter aluminum wire was wrapped about the filament. Note that to prevent contamination of the contacts, neither the aluminum wire nor any other item which would be placed in the evaporation chamber was touched with the hands.

The device was now slipped into a small amount of hydrofluoric

acid for a one-minute final cleansing and removal of oxide layers. When removed from the hydrofluoric acid, the device should have, for normal geometries, come out "dry". Any bubble of acid remaining was an indication of a defect in the previous processes and the entire pre-etch cleaning and etch cycles were repeated.

A shutter arrangement allowed exposure of the masked device only after a melt had been established and any oxides were burned off. The device itself was clamped between the teflon covered jaws of a vise-like clamp so that the face to be evaporated onto was approximately even with the edges of the clamp. A stainless steel mask was used to establish contact size.

The clamped device was now placed under the filament center and the bell jar installed. The bell jar was then evacuated to 2×10^{-6} mm of mercury pressure. The filament was turned on and gradually the current was increased until the aluminum melted and the melt formed a neat bubble on the filament. The shutter was then opened using a magnet on the outside of the jar and the current increased slightly so that the bubble, seen through the hole in the evaporation shield inside the jar, seemed to flow around the filament. The aluminum was then allowed to evaporate until the outline of the fine tungsten wire appeared in the melt. The filament was then turned off and, after a 10 minute cooling period, the bell jar was vented and the device removed. A layer of aluminum of approximately 10,000 Å was thus deposited.

Alloying

The alloying of the aluminum contact was done in a Lindberg Hevi-Duty diffusion furnace. For the aluminum contacts, the oven was

preheated by setting the controller to 500° C (20.5 mV on the chromel-alumel thermocouple meter). A nitrogen flow rate through the quartz tube of 0.1 SCFH to 1 SCFH (1 SCFH ≈ 500 cc/min) was established and a quartz boat with the device whose contacts were oriented (in so far as possible) toward the nitrogen source was inserted. When the temperature had again stabilized at 500° C, the controller was set to 620° C (the aluminum-silicon eutectic temperature is 577° C). Fifteen minutes after the controller was turned up, the oven was shut down and allowed to cool to 460° C (18 mV) at which temperature the device could be removed.

Diffusion

The n^+ contacts were made using lithium diffusion. The procedure utilized for these contacts is derived from that used by Mayer et al. (18). The contact area was first lapped with 800 grit grinding compound (it had previously been etched). After a short etch in HF, a drop of lithium dispersion[1] was placed on the surface such that the contact area was covered. The device was placed in a diffusion furnace with a nitrogen atmosphere and dried at 290° C for forty-five minutes. The oven regulator was then set at 475° C. The nitrogen flow was maintained and when the oven reached the point of regulation, it was turned off immediately. After five minutes the oven lid was raised to speed the cooling. The device was removed at 150° C. The area contacted was covered with a thick, white oxide layer which was scraped off after

---

[1] Lithium Dispersion
29% Lithium
70% Mineral Oil
1% Oleic Acid
available from Lithium Corporation of America.

loosening in methanol.

The surface underneath was generally quite rough and had to be lapped smooth with 800 grit grinding compound. The device n^+ contact area was then friction-tinned using a gallium-loaded grinding wheel until evenly coated. This provided the electrical contact to the n^+ junction. The gallium melts at just above room temperature and an indium-gallium mixture is liquid at room temperature. Thus, enough indium solder was then melted to the n^+ contact to over-saturate the gallium and provide a good mechanical contact. Leads could then be soldered to the p^+ and n^+ junction contacts with additional indium solder (Indalloy #3).

APPENDIX C

ERROR ANALYSIS

In this experimental work, as in any other similar work, a great deal of effort must be applied to the detection, analysis and correction of errors. These errors are of three categories: statistical errors, instrument errors and reading errors. In general, one is concerned only with the latter two groups and the evaluation of the total error follows in a rather straight-forward fashion. The expected error in a function y of n independent variables x_ν, each subject to expected random errors Δx_ν is given by

$$\Delta y = \left[\sum_{\nu=1}^{n} \left(\frac{\partial y}{\partial x_\nu}\right)^2 \Delta x_\nu^2\right]^{\frac{1}{2}} \quad . \qquad (C.1)$$

A summary of the approximate errors in the dc and ac measurements of this type is provided at the end of this appendix.

The measurement and analysis of the widely fluctuating noise voltages experienced in this research is quite another problem. In this case the statistical error is not only significant but, in fact, is the dominating error so that considerable effort is necessary to properly analyze the results. To determine the accuracy and validity of the results as well as to identify those measurements whose criticality could be reduced by careful selection of equipments and techniques, a more detailed study of the error was necessary.

Theoretical Noise Measurement Errors

The theoretical relative standard error α in the mean value estimate of bandwidth limited white noise is given (34) as

$$\alpha = (2\Delta f t_i)^{-\frac{1}{2}} \quad , \tag{C.2}$$

where t_i is the total integration time and Δf is the bandwidth. In this case, the rms error to be expected in a function y of n independent variables x_ν, each subject to a random fluctuation Δx_ν around its average x_ν, can be expressed as in Equation C.1,

$$\Delta y = \left[\sum_{\nu=1}^{n} \left(\frac{\partial y}{\partial x_\nu}\right)^2 \Delta x^2\right]^{\frac{1}{2}} \quad . \tag{C.1}$$

In the measurement of noise by the method used in this experimental study, the expression for equivalent noise current is

$$I_{eq} = \frac{V_1^2 - V_s^2}{V_2^2 - V_1^2} I_c - I_{eq\ z} \quad . \tag{3.3}$$

In this relation, V_s, V_1, V_2 and $I_{eq\ z}$ are considered random variables and I_c, since its readings are not subject to other than minor fluctuations, is considered fixed. The measurements of V_s, V_1 and V_2 are made with the same instruments and under similar conditions so their relative errors are considered to be equal and

$$\frac{\Delta V_s}{V_s} = \frac{\Delta V_1}{V_1} = \frac{\Delta V_2}{V_2} = \alpha \quad . \tag{C.3}$$

Then, applying Equation C.1,

$$\Delta I_{eq} = \left\{ (2\ \alpha\ I_c)^2 \left\{ \left(\frac{V_s^2}{V_2^2 - V_1^2}\right)^2 + \left[\frac{V_1^2(V_2^2 - V_s^2)}{(V_2^2 - V_1^2)^2}\right]^2 + \left[\frac{(V_1^2 - V_s^2)V_2^2}{(V_2^2 - V_1^2)^2}\right]^2 \right\} + I_{eq\ z}^2 \left(\frac{\Delta I_{eq\ z}}{I_{eq\ z}}\right)^2 \right\}^{\frac{1}{2}} \quad . \tag{C.4}$$

Now for the assumptions $V_1, V_2 \gg V_s$, $V_2 \gg V_1$ and $I_{eq} \gg I_{eq\ z}$ Equation C.4 can be reduced to the simple relation,

$$\frac{\Delta I_{eq}}{I_{eq}} \approx 2\sqrt{2}\ \alpha \quad . \tag{C.5}$$

Equation C.5 represents the minimum error. Any deviation from the assumptions above can be expected to increase this error. In this research, two wave analyzers were used and for these cases, Table IX shows the expected minimum error as 7.4% and 8.2% for the two units.

TABLE IX

EXPECTED STATISTICAL ERROR IN NOISE MEASUREMENT

Analyzer	Δf (Hz)	t_i (s)	α	$\frac{\Delta I_{eq}}{I_{eq}}$
HP 302A	6	120	.026	.074
HP 312A	200	6	.082	.082

At high device currents (and thus large noises) the limit of the calibration diode was reached and it was no longer possible to achieve the $V_2 \gg V_1$ condition. For such cases, errors were evaluated by actual substitution in Equation 3.3. Under this check it was found that the error in I_{eq} due to a 5% error in the reading of either V_1 or V_2 was about 10% for ratios of V_2 to V_1 of 2 or greater. At lower ratios, the error rose rapidly to 20% at a ratio of 1.3 and to over 100% at a ratio of 1.1. Extreme care was therefore taken to make V_2 at least twice V_1 in every possible instance. At low frequencies and high currents the ratio dropped, however readings were taken to ratios as low as 1.1 rather than leaving out these data points completely. After the data was reduced, a low frequency cutoff was established and points below this value were discarded as having excessive error.

Curve Fitting Errors

Least squares fitting programs were used for the analysis of the potential plot data, the pulse response data and for a limited number of the noise spectra. In the potential plot curves the fits were good, having an estimated error at a single point of not more than 5% with most of this error due to using the Lampert approximation for the electric field (i.e., neglecting diffusion effects). For the pulse response, the error of individual points is somewhat better being less than 2%. For the noise spectra, however, curve fitting was extremely difficult. The large amount of flicker noise and the very large scattering of data points at low frequency precluded the use of the computer in favor of the "selective weighting" of the human eye. Transparencies of the frequency sensitive factors were overlayed on the raw

noise data and fits obtained in this way. Accuracy varied with the magnitude of the noise, amount of scattering, etc., and was difficult to assess, however estimates based on successive trials is provided along with a general error summary in Table X.

TABLE X

ERROR SUMMARY

I-V Characteristics	
Statistical Error	~ 0%
Instrument Error	
Current	1%
Voltage	0.1%
Reading Error	~ 0%
Total Error*	1%
Potential Probe Measurement	
Statistical Error	~ 0%
Instrument Error	
Current (no effect on profile)	1.0%
Voltage	.1%
Distance	3%
Reading Error	
Voltage	~ 0%
Distance	3%
Analysis Error	3%
Total Error*	
Effective Length	5%
Pulse Response Measurements	
Statistical Error (noise, etc.)	3%
Instrument Error	
Voltage	2%
Time	5%
Reading Error	
Voltage	1%
Time	1%
Analysis Error	.1%
Total Error*	
Lifetime	5%
Current	5%
Noise Measurements	
Statistical Error (individual points)	
Low Current, Low Frequency	7%
Med. Current, Low Frequency	10%
High Current, Low Frequency	40%
Med. Frequency	8%
High Frequency	8%
Instrument Error	2%
Reading Error	2%
Analysis Error	
Low Current	
Plateau	10%
Lifetime	10%
High Current	
Plateau	20%
Lifetime	20%
Total Error*	
Low Current	
Plateau	15%
Lifetime	20%
Med. Current	
Plateau	20%
Lifetime	20%
High Current	
Plateau	30%
Lifetime	20%

*Total errors are based on a weighted combination of the above.

VITA

Peter Rudolph Worch

Candidate for the Degree of

Doctor of Philosophy

Thesis: AN EXPERIMENTAL INVESTIGATION OF GENERATION-RECOMBINATION NOISE IN DOUBLE-INJECTION DIODES

Major Field: Electrical Engineering

Biographical:

Personal Data: Born in Binghamton, New York, September 15, 1935, the son of Mr. and Mrs. J. Rudolph Worch.

Education: Attended Technical High School in Binghamton, New York. Graduated from Union College, Schenectady, New York with the Bachelor of Science degree in Electrical Engineering in June, 1957. Entered military service (U.S. Air Force) in 1957, serving continuously to the present. Attended Oklahoma State University from January, 1963 to January, 1965 and received the Master of Science degree in Electrical Engineering in May, 1965. Completed extension graduate work under the University of Southern California (Aerospace Safety Division) at Tachikawa, Japan in 1965 and 1967. Entered Oklahoma State University in January, 1968 and completed requirements for the Doctor of Philosophy degree at Oklahoma State University in May, 1970.

Professional Experience: Worked as an Electrical Engineer with General Electric Company from June, 1957 through July, 1957. Served as Air Electronics Officer in the Tactical Air Command and the Military Air Transport Service from 1957 through 1960. Appointed as Air Electronics Staff Officer with Air Defense Command until 1963. Worked as Chief, Communications Systems Maintenance Branch and as Chief, Systems Engineering Division with Headquarters, Far East Communications Region from January, 1965 through November, 1967. Current rank is Major in the United States Air Force.

Professional Memberships: Institute of Electrical and Electronics Engineers, Eta Kappa Nu.